ACS Infectious Diseases

Article

JMX0207, a niclosamide derivative with improved pharmacokinetics, suppresses Zika virus infection both in vitro and in vivo

Zhong Li, Jimin Xu, Yuekun Lang, Xiaoyu Fan, Lili Kuo, Lianna D'Brant, Saiyang Hu, Subodh Samrat, Nicole Trudeau, Anil Tharappel, Natasha Rugenstein, Cheri Koetzner, Jing Zhang, Haiying Chen, Laura Kramer, David Butler, Qing-Yu Zhang, Jia Zhou, and Hongmin Li

ACS Infect. Dis., **Just Accepted Manuscript** • DOI: 10.1021/acsinfecdis.0c00217 • Publication Date (Web): 31 Aug 2020

JMX0207, a niclosamide derivative with improved pharmacokinetics, suppresses Zika virus infection both *in vitro* and *in vivo*

Zhong Li[#], Jimin Xu[#], Yuekun Lang, Xiaoyu Fan, Lili Kuo, Lianna D'Brant, Saiyang Hu, Subodh Kumar Samrat, Nicole Trudeau, Anil M. Tharappel, Natasha Rugenstein, Cheri A Koetzner, Jing Zhang, Haiying Chen, Laura D Kramer, David Butler, Qing-Yu Zhang, Jia Zhou*, Hongmin Li*

[1] Wadsworth Center, New York State Department of Health, 120 New Scotland Ave, Albany, NY 12208, USA

[2] Chemical Biology Program, Department of Pharmacology and Toxicology, University of Texas Medical Branch, Galveston, TX 77555, USA

[3] Department of Pharmacology and Toxicology, College of Pharmacy, University of Arizona, Tucson, AZ 85721, USA

[4] The Neural Stem Cell Institute, 1 Discovery Drive, Rensselaer, NY 12144, USA

[5] Department of Biomedical Sciences, School of Public Health, University at Albany, Albany, NY 12201, USA

Abstract

Flaviviruses causes significant human disease. Recent outbreaks of the Zika virus highlight the need to develop effective therapies for this class of viruses. Previously we identified niclosamide as a broad-spectrum inhibitor for flaviviruses by targeting the interface between viral protease NS3 and its cofactor NS2B. Here, we screened a small library of niclosamide derivatives and identified a new analogue with improved pharmacokinetic properties. Compound **JMX0207** showed improved efficacy in inhibition of the molecular interaction between NS3 and NS2B, better inhibition of viral protease function, and enhanced antiviral efficacy in cell-based antiviral assay. The derivative also significantly reduced Zika virus infection on 3D mini-brain organoids derived from pluripotent neural stem cells. Intriguingly, the compound significantly reduced viremia in a ZIKV animal model. In summary, a niclosamide derivative **JMX0207** was identified which shows improved pharmacokinetics and efficacy against Zika virus both *in vitro* and *in vivo*.

Keywords: Flavivirus, Zika virus, Dengue virus, antiviral, protease inhibitor

The genus *Flavivirus* is composed of more than 70 viruses. Many flaviviruses, including the four serotypes of the Dengue virus (DENV1-4), the West Nile virus, and the Zika virus (ZIKV or ZK) cause serious human diseases. Recently, significant ZIKV outbreaks have occurred worldwide.[1-5] ZIKV is transmitted to humans primarily through bites from infected *Aedes* species mosquitoes, but may also be transferred prenatally or through sexual activities or blood transfusions.[6-9] ZIKV infection is associated with devastating diseases, including Guillain-Barré syndrome, a rare neurological syndrome, and congenital Zika syndrome, which is manifested by microcephaly, brain abnormalities, and other central nervous system malformations.[1-5] In addition, ZIKV persists in neuronal and/or reproductive tissues of animals for up to 60 days after viral infection, leading to severe damage.[10-12] Currently there is neither a safe and effective vaccine nor a specific therapy for ZIKV. Although a DENV vaccine is recently approved, it is effective in children between 9 and 16-year-old, and posts increased risk for naïve children due to antibody-dependent enhancement.[13] Therefore, there is an unmet medical need to develop direct antivirals against flaviviruses.

The flavivirus genome encodes a single open reading frame, from which a polyprotein precursor is expressed.[14-16] The polyprotein precursor is post-translationally processed into 10 mature proteins, including three structural and seven non-structural proteins, by viral and host proteases in a sequential manner.[14-15] The viral protease is a heterocomplex composed of viral NS3 protein and its viral co-factor NS2B.[14] The viral protease has been considered a highly promising drug target.[14, 17-19] Various strategies have been used to develop protease inhibitors. The majority of efforts have been focused on the viral protease active site,[13,16-18] but with limited success in finding inhibitors with *in vivo* efficacy.[20] Recently, alternative strategies to target the NS2B-NS3

interaction[21-22] and allosteric sites[23-25] have led to identification of potent protease inhibitors with *in vivo* efficacy against Zika virus.

Previously, we developed a split luciferase complementation (SLC)-based high throughput screening strategy to identify inhibitors targeting the NS2B-NS3 interface of DENV2 (DN2).[21] Niclosamide was found to be a broad-spectrum inhibitor for flaviviruses by targeting the interface between viral protease NS3 and its co-factor NS2B, leading to accumulation of non-functional viral polyprotein precursor.[21] In addition, niclosamide was found to interfere with virus entry[26] and endosomal acidification.[27] Moreover, niclosamide was found as a broad-spectrum antiviral against multiple viruses including SARS Cov-2, the causing agent of current COVID-19 pandemic.[28] Unfortunately, niclosamide did not show appreciable *in vivo* antiviral efficacy towards ZIKV (data not shown), possibly due to its poor pharmacokinetic properties.[26, 29]

In this work, we screened a small library of niclosamide derivatives. We found that one derivative, **JMX0207**, showed improved efficacy in inhibition of the NS2B-NS3 interaction, better inhibition of viral protease function, and enhanced antiviral efficacy in cell-based antiviral assay, compared to niclosamide. **JMX0207** was also found to significantly reduce ZIKV infection on a 3D mini-brain organoid model derived from pluripotent neural stem cells. Intriguingly, **JMX0207** significantly improved the pharmacokinetic properties and markedly reduced viremia in a ZIKV animal model.

Results

Synthesis and screening of Niclosamide derivatives.

Niclosamide was originally used as an anthelmintic drug. It was also found to have anti-cancer and antibacterial activities.[30-34] We previously developed a small library composed of 62 niclosamide derivatives for other purposes.[33-38] These niclosamide analogs have been

resynthesized in-house following our published procedures for antiviral evaluation. To identify niclosamide derivatives that have equal or better antiviral efficacy and improved pharmacokinetic properties, we used our SLC-based NS2B-NS3 interaction assay to screen this library, with niclosamide as a control.

Table 1. IC_{50},[a] EC_{50}, CC_{50} (all in μM), and therapeutic index (TI) of niclosamide derivatives.

Compound[b]	Structure	$IC_{50\text{-}SLC\text{-}}$ (DN2)	$IC_{50\text{-pro}}$ (DN2)	$EC_{50\text{-DN2}}$ (A549)	$EC_{50\text{-ZK}}$ (A549)	CC_{50} (A549)	TI[c] (DN2)	TI (ZK)
Niclosamide	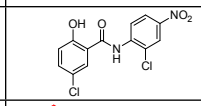	2.0	21.6	0.55	0.48	4.8	8.7	10.0
HJC0114	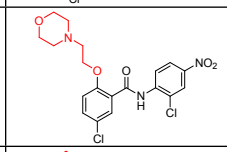	18.4	33.6	>30	>30	>200		
HJC0125	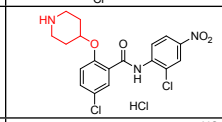	16.3	44.5	0.21	0.15	50.2	239	335
HJC0308	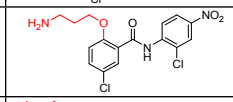	4.9	39.7	1.4	6.2	17.7	12.6	2.8
HJC0365	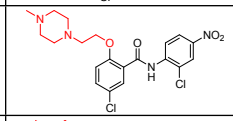	13.2	>60	6.4	6.0	177	27.6	29.5
HJC0381	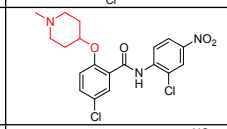	10.8	25.9	1.2	3.9	91.1	76	23.3
HJC0390	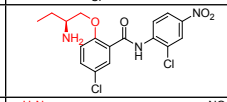	6.0	46.5	0.43	<0.1	30.1	70	>300
HJC0431	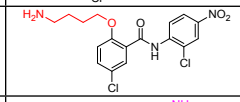	3.1	34.0	2.2	0.36	28.4	13	79
HJC0129	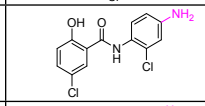	9.6	11.3	>30	>30	176		
HJC0140	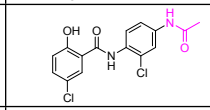	9.4	25.5	>30	>30	>200		
HJC0149	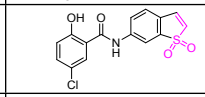	18.6	20.3	0.9	1.1	241	268	219
JMX0207	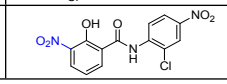	1.3	8.2	0.31	0.30	31.9	103	106

[a] $IC_{50\text{-}SLC}/IC_{50\text{-}pro}/EC_{50}/CC_{50}$: Compound concentrations required to reduce 50% of the split luciferase complementation (SLC) signal, protease activity, virus production, and cell viability, respectively. [b]Original

compound names from literature and this work. According to their structures, these compounds can be classified into three groups, colored as red, magenta, and blue, respectively. [c] TI, therapeutic index (TI) defined as CC_{50}/EC_{50}. All values are in micromolar (μM) except TI. DN2, Dengue virus serotype 2; ZK, Zika virus.

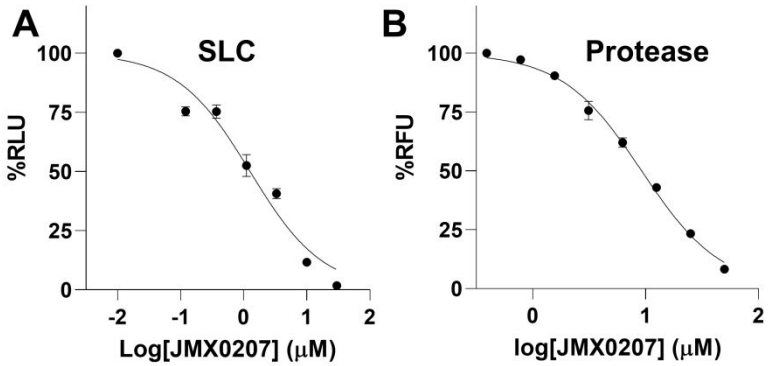

Figure 1. Inhibition of the NS2B-NS3 interactions and protease activity. (A) Dose-dependent inhibition of SLC upon binding of NLuc-NS2B$_{49-66}$ to GST-CLuc-NS3 by **JMX0207**. N=3. **(B)** Dose-response inhibitions of the DENV2 His-NS2B/His-MBP-NS3 protease activity by **JMX0207**. N=3. In both (A) and (B), DMSO control was set as 100%. The values represent means ± standard deviation (S.D.) in all panels.

Eleven out of 62 niclosamide derivatives showed dose-responsive inhibition of the interaction between viral NS3 protease and its cofactor NS2B, with $IC_{50\text{-}SLC}$ values lower than 30 μM, the highest concentration tested ($IC_{50\text{-}SLC}/IC_{50\text{-}pro}/EC_{50}/CC_{50}$: compound concentrations required to reduce 50% of the split luciferase complementation signal, protease activity, virus production, and cell viability, respectively) (**Table 1, Figure 1**). The derivatives identified included seven compounds with *O*-alkylamino chains, one compound with 3-NO_2 instead of 5-Cl on the salicylic ring, and three compounds with modifications on the nitro group of the aniline moiety. Of these active derivatives, compounds **HJC0308** with 3-aminopropoxy moiety, **HJC0431** with 4-aminobutoxy moiety, and **JMX0207** with 3-NO_2 group showed comparable or

better inhibition of the NS2B-NS3 SLC with $IC_{50\text{-}SLC}$ values of 4.9 μM, 3.1 μM and 1.3 μM, respectively, compared to niclosamide.

Inhibition of the NS2B-NS3 protease activity.

We next evaluated the inhibition efficacy of these positive derivatives against the viral NS2B-NS3 protease function as previously described.[21] Previously, we generated two versions of the NS3 protease, the NS3 protease domain refolded from inclusion bodies and a soluble version of the NS3 protease domain fused to maltose-binding protein (MBP).[21-22] Our data showed that the refolded and MBP-tagged NS3 proteins have indistinguishable protease activities when transactivated by co-factor NS2B. In this work, we used both versions to characterize the inhibitors and found that the IC_{50} values determined from both versions were similar. Therefore, only values for the refolded NS3 were shown. As shown in **Table 1**, most active compounds in SLC assay except **HJC0365** still showed inhibition against the viral NS2B-NS3 protease activity. However, we found that there seemed to be no strict correlation between $IC_{50\text{-}SLC}$ and $IC_{50\text{-}pro}$ values. This is not surprising because niclosamide is a known luciferase inhibitor.[39] The SLC inhibition is an indirect readout of the NS2B-NS3 interactions. Direct inhibition of luciferase activity and/or direct inhibition of luciferase complementation in addition to inhibition of NS2B-NS3 interaction may account for the poor correlation between $IC_{50\text{-}SLC}$ and $IC_{50\text{-}pro}$ values. While $IC_{50\text{-}SLC}$ is a poor indicator of inhibition efficacy of the NS2B-NS3 interactions, it remains a valuable indicator to eliminate compounds if they failed to inhibit SLC.

Among these derivatives, compounds **HJC0140** with 4′-acetamido group ($IC_{50\text{-}pro}$ = 25.5 μM), **HJC0149** with benzo[*b*]thiophene 1,1-dioxide moiety ($IC_{50\text{-}pro}$ = 20.3 μM) and **HJC0381** with (1-methylpiperidin-4-yl)oxy moiety ($IC_{50\text{-}pro}$ = 25.9 μM) maintained the same level of potency, while compounds **HJC0129** with 4′-NH_2 group ($IC_{50\text{-}pro}$ = 11.3 μM) and **JMX0207** with

3-NO_2 group ($IC_{50\text{-}pro}$ = 8.2 μM) showed nearly or more than 2-fold improvement in inhibition of the viral NS2B-NS3 protease activity, compared to niclosamide ($IC_{50\text{-}pro}$ = 21.6 μM) (**Table 1 , Figure 1**). Taken together, the three compounds **HJC0129** ($IC_{50\text{-}SLC}$ = 9.6 μM and $IC_{50\text{-}pro}$ = 11.3 μM), **HJC0140** ($IC_{50\text{-}SLC}$ = 9.4 μM and $IC_{50\text{-}pro}$ = 25.5 μM), and **JMX0207** ($IC_{50\text{-}SLC}$ = 1.3 μM and $IC_{50\text{-}pro}$ = 8.2 μM) showed potent inhibitory activity against the NS2B-NS3 interactions in both NS2B-NS3 SLC and NS2B-NS3 protease assays.

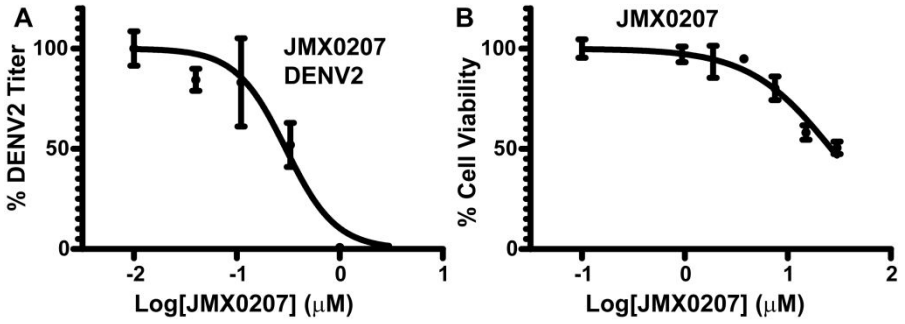

Figure 2. JMX0207 inhibits DENV. (A) Dose-dependent inhibition of DENV2 infectivity by **JMX0207**. N=3. (**B**) Cell viability assay. A549 cells were incubated with various concentrations of **JMX0207** and then assayed for viability at 48 hrs post-incubation. N=3. Error bars in both panels represent the standard deviations at each concentration.

Inhibition of DENV2 viral replication.

A viral plaque reduction assay was performed next to evaluate the antiviral efficacy of these derivatives. Human lung carcinoma A549 cells were infected with DENV2 in the presence of a concentration series of derivatives or a dimethyl sulfoxide (DMSO) control, and viral titers were measured at 48 hrs post-infection, as described previously.[21-22, 40] Our results indicated that eight out 11 active derivatives showed appreciable antiviral efficacy with $EC_{50\text{-}DN2}$ less than 30 μM (**Table 1**). The best derivative, **JMX0207,** showed slightly improved antiviral efficacy ($EC_{50\text{-}DN2}$ of 0.31 μM), compared to niclosamide ($EC_{50\text{-}DN2}$ of 0.55 μM) (**Figure 2A**).

The observed antiviral activity could result from compound's cytotoxicity. To address this concern, we next measured the compound cytotoxicity CC_{50} using a WST-8 cell proliferation assay, as we described previously.[21] As shown in **Table 1** and **Fig. 2B**, the majority of these derivatives showed improved CC_{50} and therapeutic index (defined as CC_{50}/EC_{50}), compared to niclosamide.

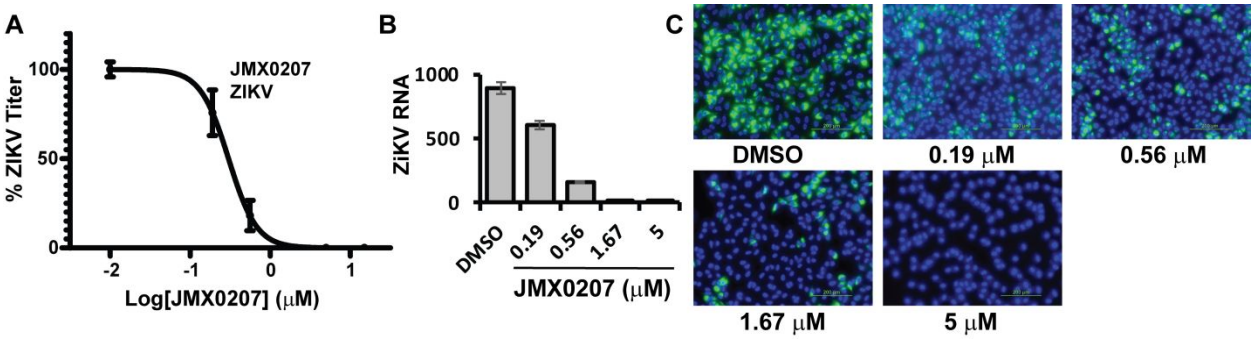

Figure 3. JMX0207 inhibits ZIKV. (A) Dose-dependent inhibition of ZIKV infectivity. N=3. (**B**) qRT-PCR analysis of inhibition of viral RNA from ZIKV-infected A549 cells by **JMX0207**. N=3. Error bars in panels (**A**) and (**B**) represent the standard deviations at each concentration. (**C**) Immunofluorescence assay of inhibition of viral protein production by **JMX0207**, using pan-flavivirus anti-E 4G2 antibody (green) (ATCC).

Inhibition of ZIKV replication.

Our previous studies indicated that niclosamide is a broad-spectrum inhibitor against multiple flaviviruses[21]. To determine the antiviral spectrum of the derivatives, we evaluated the antiviral potency of the derivatives against ZIKV. Our results showed that the derivatives were also potent inhibitors against ZIKV, with $EC_{50\text{-}ZK}$ values comparable to those for DENV2 (**Table 1**, **Figure 3A**). Similarly, **JMX0207** showed better inhibition efficacy towards ZIKV than niclosamide (**Figure 3A**).

JMX0207 treatment leads to reductions in viral RNA yield and protein production.

Among the derivatives, **JMX0207** showed improved efficacy in almost all categories (**Table 1**), compared to niclosamide. Therefore, we chose **JMX0207** to further characterize whether **JMX0207** treatment led to inhibition of viral RNA synthesis and viral protein production, using qRT-PCR and immunofluorescence assay (IFA), respectively. Our results indicated that **JMX0207** significantly reduced the ZIKV RNA copy number in a dose-dependent manner (**Figure 3B**). Using a pan flavivirus anti-E antibody 4G2, we conducted an IFA to demonstrate that **JMX0207** greatly reduced ZIKV antigen production in A549 cells in a dose-dependent manner (**Figure 3C**), presumably because of inhibition of viral replication.

Overall, these experimental results indicated that **JMX0207** showed improved anti-protease, antiviral, and cytotoxicity properties, compared to niclosamide. **JMX0207** treatment results in inhibition of viral infectivity, viral RNA replication, and viral protein production, and is a broad-spectrum antiviral for flaviviruses.

JMX0207 inhibits viral production in cells relevant to ZIKV pathogenesis.

We next used human induced pluripotent stem cell (iPSC)-derived neural progenitor cell (HNPC) [21, 41] to investigate whether **JMX0207** is an effective inhibitor in human primary cells demonstrated to be relevant to ZIKV pathogenesis.[42-46] As shown (**Figure 4A & 4B**), **JMX0207** effectively inhibited ZIKV protein expression and RNA synthesis in HNPC in dose-dependent manner. Overall, these experiments demonstrate that **JMX0207** is an effective antiviral in neural progenitor cells relevant to ZIKV infection.

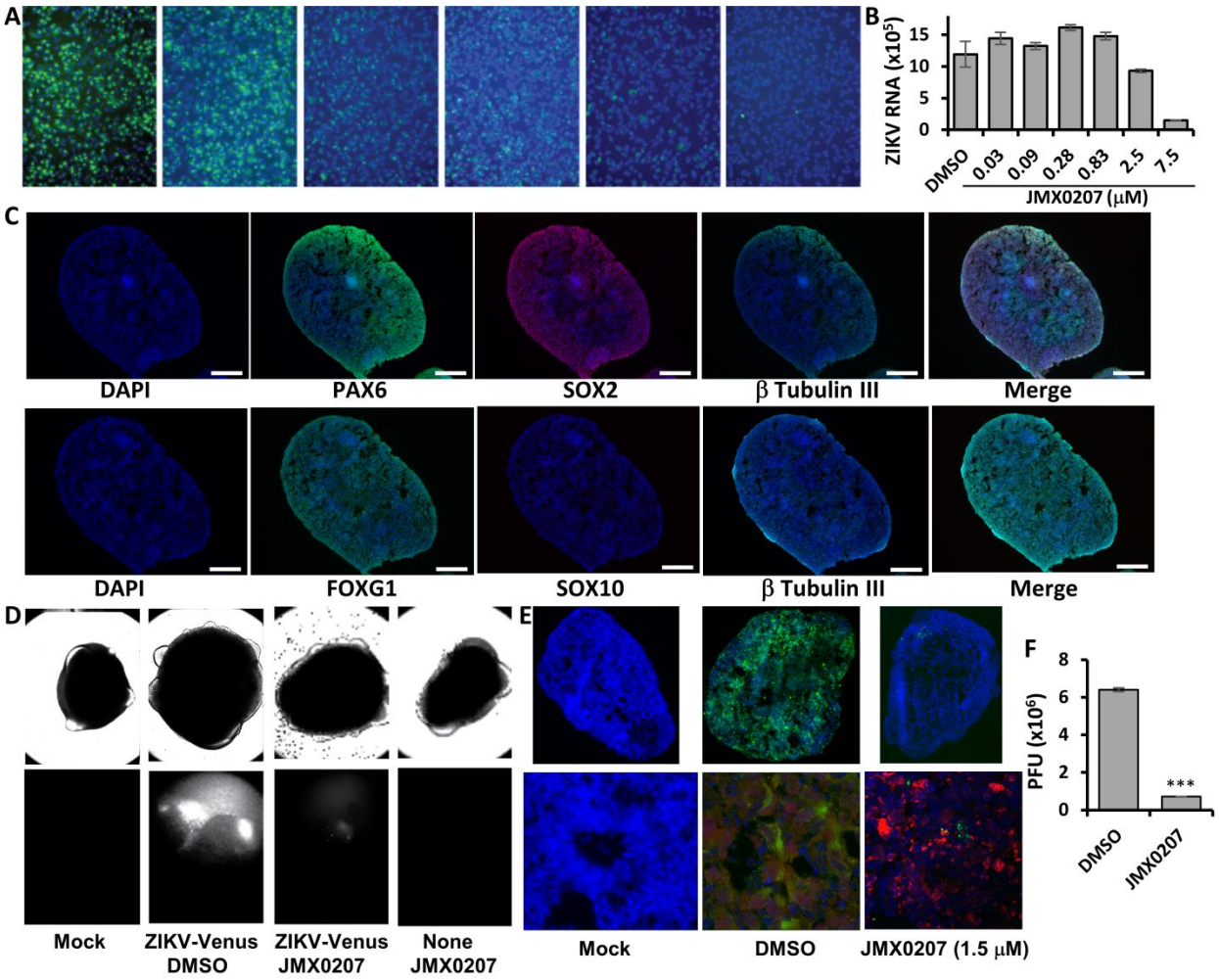

Figure 4. Inhibition of ZIKV in cells relevant to ZIKV. (A) Immunofluorescence assay (IFA) of inhibition of viral protein expression in human neural progenitor cells by **JMX0207**, using pan-flavivirus anti-E 4G2 antibody (green) (ATCC). Nuclei (blue) was stained in all IFA assays by the Hoechst stain solution. (**B**) qRT-PCR analyses of inhibition of viral RNA from ZIKV-infected human neural progenitor cell (HNPC) by **JMX0207**. N=3 (**C**) ZIKV organoid infected with ZIKV-Venus. The 3D organoids were infected with PBS (Mock), or ZIKV untreated (DMSO), or ZIKV treated with **JMX0207**, or Mock treated with **JMX0207**. Upper panel, bright field image of intact organoids. Lower panel, Venus fluorescence image (excitation 515 nm, emission 528 nm) of the intact 3D organoids. (**D**) Forebrain reginal specification of organoids. Organoids were stained

positive for forebrain identity markers PAX6 (green, upper panel), FOXG1 (green, lower panel) and SOX2 (Red (Magenta after merge with DAPI (Blue)), upper panel) at 20 days. The sections were stained positive for general neuronal marker TUJI (cyan, upper and lower panels) and were negative for SOX10 (Red, lower panel). DAPI-merged data were shown. Nuclei (DAPI, Blue); scale bar 200μm. (**E**) Slices of organoid infected with ZIKV PRVABC59. The 3D organoids were infected with PBS (Mock), or ZIKV untreated (DMSO), or ZIKV treated with **JMX0207**. Upper panel, IFA using anti-E 4G2 antibody (green); blue, DAPI. Lower panel, details of signature rosette region of the 3D organoids (Mock) or infected region (DMSO/ZIKV and **JMX0207**/ZIKV). Red: Pax6. (**F**) ZIKV production from the 3D organoids at 5 dpi. Culture supernatants were collected, and virus production was quantified by PFU assay. N=3. Error bars in panels (**B**) and (**F**) represent the standard deviations at each concentration.

JMX0207 protects 3D mini-brain organoid from ZIKV infection.

Newborns from mothers with ZIKV infection during pregnancy have significantly increased risk of developing microcephaly, a birth defect where a baby has smaller than normal head circumference. Babies born with microcephaly may develop many brain-related or other neurological problems. Recently, neural stem cell-derived 3D cerebral organoids were used to dissect ZIKV pathogenesis and anti-viral development.[45, 47-49] Compared to the cultured 2D monolayer cells, the 3D brain organoids can better represent the composition, diversity and organization of cell types found in the developing human brain.

Therefore, we used the 3D mini-brain organoid model to further investigate whether **JMX0207** can protect against ZIKV-associated neurological damage. Induced pluripotent stem cells (iPSC) derived from a healthy control (Male, Caucasian) were differentiated using an

established protocol to generate region-specific organoids patterned to resemble the dorsal forebrain (**Figure 4C**).[50] Organoids were stained positive for forebrain identity markers PAX6 (dorsal forebrain progenitors; upper panel), FOXG1 (lower panel) and SOX2 (neural ectoderm marker, upper panel) at 20 days. The sections were stained positive for general neuronal marker TUJI (neuron-specific class III β-tubulin; upper and lower panels) and were negative for SOX10 (Neural crest, Red, lower panel).

To evaluate if **JMX0207** protects organoids from ZIKV infections, we first generated a full-length infectious ZIKV clone expressing Venus fluorescent protein (ZIKV-Venus) (details to be published elsewhere). At day 20, the organoids displayed signature features of forebrain, including neural rosettes (**Figure 4C-E**), and were pre-treated with **JMX0207** (1.5 μM) or DMSO control. At day 20, the organoids were infected with either Mock or ZIKV strain PRVABC59 or ZIKV-Venus, at an estimated multiplicity of infection (MOI) of 1 in the presence of 1.5 μM **JMX0207** or DMSO control. ZIKV infection was quantified by a plaque forming unit (PFU) assay at 5 dpi and by fluorescence imaging at 7 dpi, respectively. Our results showed that **JMX0207** at 1.5 μM concentration did not have any toxic effect on the 3D organoids, which remained intact and unchanged in morphology (**Figure 4D**). Compared to DMSO control, **JMX0207** treatment completely abolished ZIKV infection in the 3D organoid (**Figure 4D**).

The 3D mini-brain organoids were sliced for immunostaining to investigate the antiviral effects of **JMX0207** (**Figure 4E**). As shown, untreated organoids (DMSO) were infected with ZIKV throughout all layers (**Figure 4E**). In contrast, **JMX0207** treatment nearly completely protected the organoids from ZIKV infection (**Figure 4E**). Moreover, ZIKV production was also significantly inhibited by **JMX0207** treatment (**Figure 4F**). Collectively, the results indicated that

JMX0207 is an effective inhibitor to protect developing human cortical tissue from ZIKV infection.

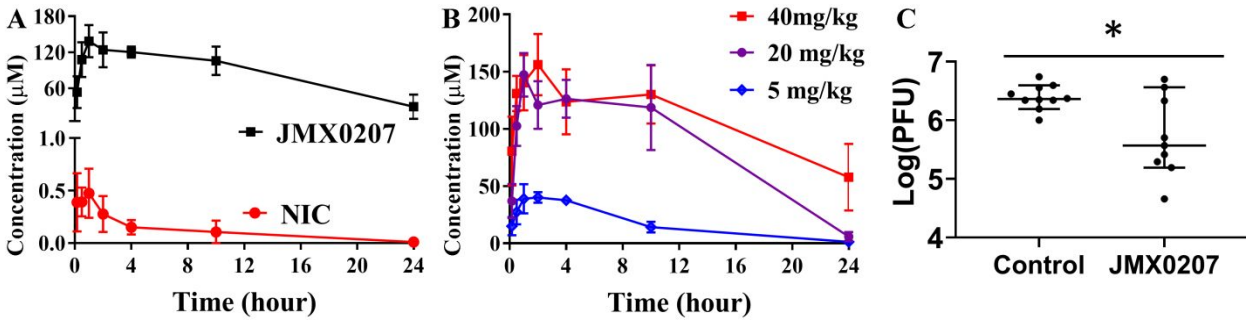

Figure 5. *In vivo* antiviral activity of JMX0207 against ZIKV. (A) Pharmacokinetic study of niclosamide and **JMX0207**. Adult female B6 mice were given a single oral dose of either niclosamide or **JMX0207** at 40 mg/kg. Plasma was obtained at various times after dosing. Both niclosamide and JMX0207 were extracted from the plasma and then analyzed by LC-MS/MS as described in the Methods. N=4. **(B)** Pharmacokinetic study of **JMX0207** at different doses. N=4-5. The values in panels (**A**) and (**B**) represent means ± S.D. (**C**) Viremia was detected by a plaque forming unit (PFU) assay on day 3 post-infection of ZIKV with a dose of 1.7×10^5 PFU/mouse in four-week-old A129 mice, which were treated with vehicle or **JMX0207** though oral gavage. Difference between **JMX0207** (N=10) or vehicle (N=10) treatment was analyzed by using the unpaired, two-tailed t-test. *, P=0.0081. Error bars represent data range of median with 95% confidence interval.

JMX0207 shows improved pharmacokinetic properties.

We next evaluated whether **JMX0207** has favorable pharmacokinetic properties using a mouse model. As shown in **Table 2** and **Figure 5A**, **JMX0207** displayed much better pharmacokinetic properties than the lead compound niclosamide. In contrast to niclosamide, which had a short $T_{1/2}$ and low C_{max} (0.6 μM), when given to B6 mice orally at 40 mg/kg **JMX0207** had

an excellent pharmacokinetic profile with C_{max} of 145 μM **(Table 2)**, which was much higher than the EC_{50} (0.3 μM) required to inhibit ZIKV. The longer $T_{1/2}$ (~11 h) was also more favorable to ensure less frequent drug administration to infected animals. Further pharmacokinetic study with different doses of JMX0207 indicated that the plasma drug concentration remained at the same level after the dose was reduced to 20 mg/kg (**Figure 5B**). More importantly, mice with repeated oral dosing at 40 mg/kg/day for 7 days did not display any sign of toxicity (N=6). These results indicate good bioavailability and low toxicity for the derivative **JMX0207**.

Table 2. Pharmacokinetic properties of niclosamide and JMX0207

	T_{max} ±S.D.[a] (h)	C_{max} ±S.D. (μM)	$T_{1/2}$ ± S.D. (h)	$AUC_{0\rightarrow\infty}$ ± S.D.
Niclosamide	0.7±0.4	0.6±0.1	4.6±1.0	3.5±0.8
JMX0207	1.2±0.5	145±18	11±6.8	2719±1018

[a] S.D., standard deviation

JMX0207 reduces viremia in a ZIKV mouse model.

Finally, we evaluated the *in vivo* antiviral efficacy using a viremia mouse model, as we described previously.[51-52] Our data showed that **JMX0207** treatment at 20 mg/kg/day resulted in a significant reduction in ZIKV-induced viremia in the A129 mice inoculated with 1.7×10^5 PFU PRVABC59 ZIKV/mouse compared to the vehicle control (**Figure 5C**). Overall, the results indicated that **JMX0207** not only inhibited viral replication *in vitro* but also significantly reduced viremia in an *in vivo* animal model.

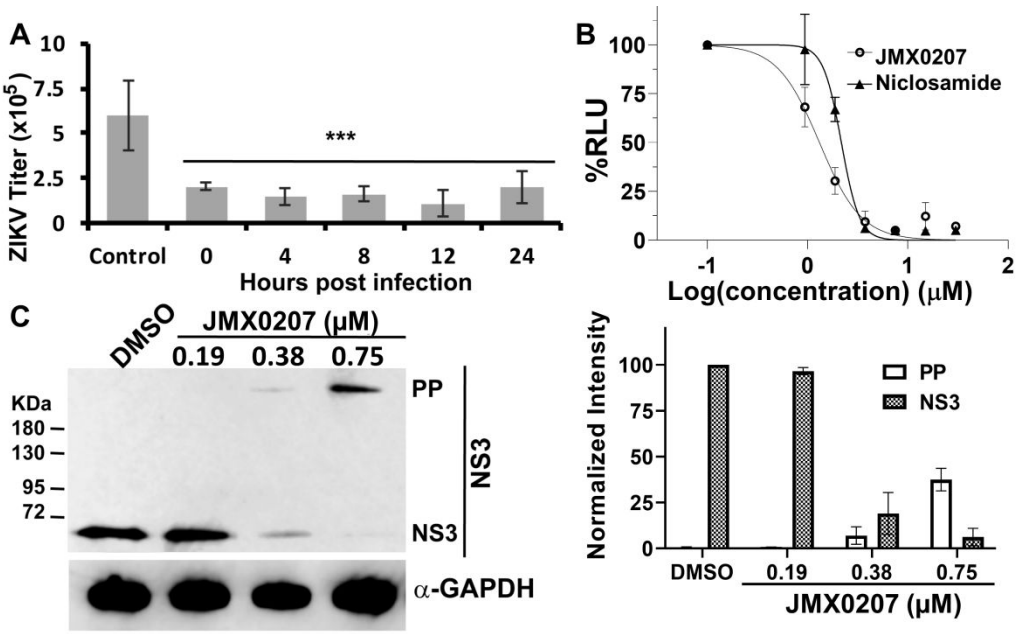

Figure 6. Mechanism of action studies. (**A**) Time of addition. **JMX0207** (0.75 μM) was added at indicated time points post-infection. Viral titers were quantified using plaque forming assay 48 hrs post-infection. DMSO was added to control. N=3. ***, p<0.001. (**B**) Dose-dependent inhibition of DENV2 replicon by niclosamide and **JMX0207**. N=3. **(C)** WB analysis of dose response inhibition of ZIKV NS3 production by **JMX0207** treatment (left). Right, Band intensities of PP and NS3 normalized to the GAPDH control (N=3). Pre-seeded A549 cells in 6-well plate were treated with **JMX0207** or DMSO control and infected with ZIKV with MOI of 0.1, as described previously.[21] At 48 hrs post-infection, cells were washed, harvested, and protected by protease inhibitor cocktail prior to lysis by SDS-PAGE loading buffer. Upon incubation at 95 ºC for 10 min, sample was subjected to Western blot analysis with anti-ZIKV NS3 (GTX133309, GeneTex, Inc.) and anti-GAPDH (CB1001, EMD Millipore) as primary antibodies. Error bars in all panels represent the standard deviations at each condition.

JMX0207 is effective post-infection.

Antiviral inhibitors are generally divided into two categories, entry and post-entry (replication), respectively. To determine the mode of action, we first performed a time of addition experiment by adding JMX0207 at different time points post-infection (**Figure 6A**). Our results showed that **JMX0207** was equally effective in reducing ZIKV titer even at 24 hrs post-infection. The results indicated that **JMX0207** inhibited viral replication instead of viral entry, which agrees with our hypothesis that **JMX0207**, as a protease inhibitor, attenuates viral production in the post-entry replication stage.

JMX0207 inhibits viral replication using a DENV2 replicon cell line.

To further investigate the mechanism of action, we next used a DENV2 replicon cell line[53] to investigate if **JMX0207** inhibited flavivirus replication without an entry step. Our results indicated that both niclosamide and **JMX0207** showed dose-responsive inhibition of DENV2 replication using the DENV2 replicon cell line (**Figure 6B**). **JMX0207** has slightly improved antiviral efficacy ($EC_{50\text{-}DN2}$ of 1.1 μM) compared to niclosamide ($EC_{50\text{-}DN2}$ of 2.0 μM) (**Figure 6B**). Overall, the results indicate that **JMX0207** is an effective antiviral to inhibit viral replication instead of entry.

JMX0207 treatment inhibits viral polyprotein precursor (PP) processing

We carried out Western blot (WB) analysis using an antibody recognizing ZIKV NS3 protein (**Figure 6C**). Our results showed that **JMX0207** treatment led to dose-dependent reduction of viral NS3 protein production, presumably due to inhibition of viral production by **JMX0207**. In addition to reduced NS3 protein production, we observed dose-dependent increase of a protein with high molecular weight (MW) (**Figure 6C**). It was known from our previous studies that the high MW protein is the unprocessed viral polyprotein precursor (PP) which can be recognized by the anti-NS3 antibody[21, 23]. The results are consistent with the mechanism by which **JMX0207**

inhibits viral protease function, leading to inhibition of viral PP processing, accumulation of non-functional viral PP, and finally virus reduction.

JMX0207 directly binds to the NS2B-NS3 interface.

As a niclosamide derivative, **JMX0207** is expected to directly bind to the viral NS3 protease, as did niclosamide.[21] To demonstrate binding, we first carried out a protein thermal shift assay (PTSA). Our data indicated that the binding of **JMX0207** stabilized the viral NS3 protease, leading to a 0.75 ºC increase in T_m of the viral protein. The data suggests that **JMX0207** directly binds the viral NS3 protease.

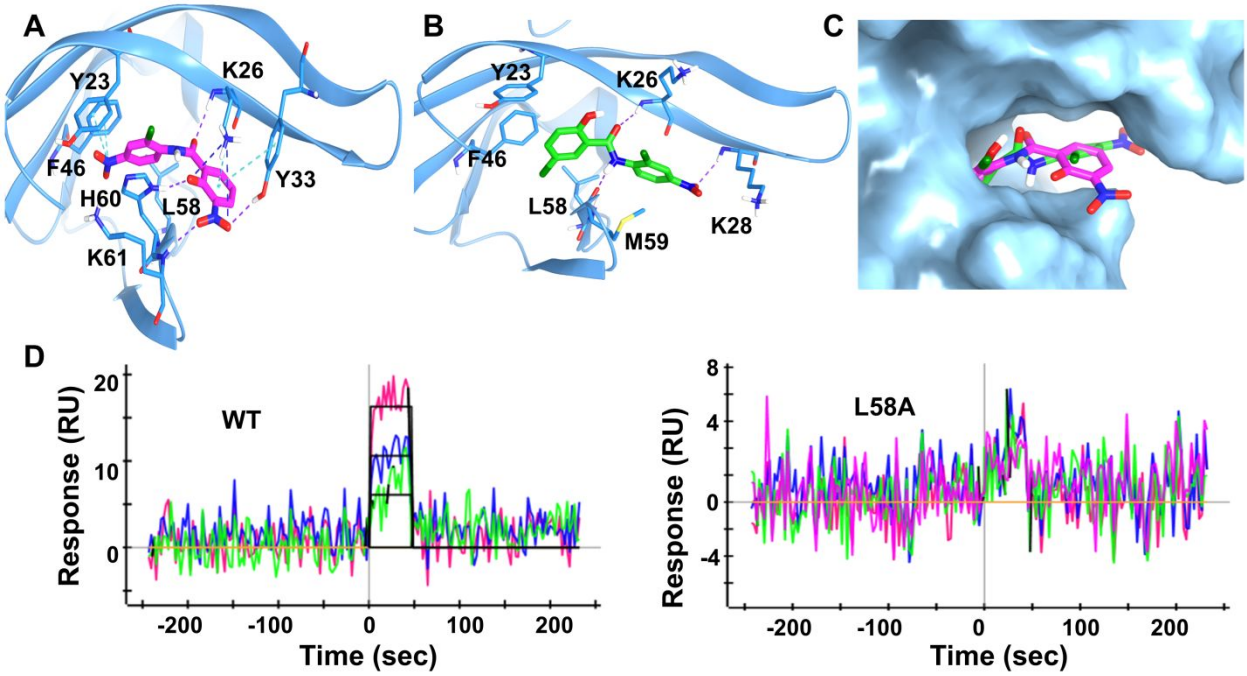

Figure 7: Docking and mutagenesis. (**A**) Predicted docking pose of **JMX0207** (magenta) docking into NS3pro of DENV2 (PDB Code: 2FOM). NS3pro is in blue ribbon representation and binding site key interaction residues are highlighted in stick presentation. π cation and π stacking are shown as cyan dotted lines, H-bond in purple and salt bridge in blue. (**B**) Predicted binding pose of Niclosamide (green) docked into NS3pro of DENV2. H-bond is shown as purple dotted lines. (**C**) **JMX0207** and Niclosamide superimposed at the predicted binding site, in surface representation.

JMX0207 is shown as magenta sticks and Niclosamide in green. (D) Representative SPR analysis of **JMX0207** binding to the MBP-NS3 protease wild-type and mutant L58A.

To investigate the molecular interaction between JMX0207 and viral NS3 protease, we docked **JMX0207** to the NS3 protease structure of DENV2 (PDB ID: 2FOM) using Induced Fit Docking (IFD) protocol, as we describe previously[21-22]. The docked pose (**Figure 7A**) depicted **JMX0207** can be well docked into the same 2B53 pocket identified from previous study[21]. One NO_2 group of JMX0207 interacts with Y23 and F46 through π cations, while another NO_2 group forms H-bonds with Y33 and K61 and a salt bridge with K26. The phenyl ring on one side of JMX0207 interacts with L58 through hydrophobic interaction, and the other phenyl ring engages with Y33 with π- π interaction. The phenol forms an H-bond with H60. The O atom on carbonyl group of JMX02027 forms an additional H-bond with K26 to further stabilize the binding. We superimposed the IFD docking pose of JMX0207 and the IFD docking pose of niclosamide. The overlay analysis demonstrates that **JMX0207** binds at the 2B53 pockets on NS3 protease of ZIKV in a similar manner to that of niclosamide (**Figure 7B,C**), while an additional nitro group of **JMX0207** also forms critical binding interactions with the protease.

To further investigate JMX0207 binding to viral NS3 protein, we used surface plasmon resonance (SPR) to measure the binding affinity of **JMX0207** to the viral NS3 protease. Because we previously generated several MBP-NS3 mutants,[22] we used MBP-NS3 fusion protein in the SPR analyses for better comparison. As shown in **Figure 7D**, **JMX0207** bound the viral NS3 protease with a binding affinity of 1.1 μM. Collectively, our data demonstrated that **JMX0207** directly binds to the viral NS3 protease, with an affinity better than that for niclosamide (6.4 μM).[21]

In a previous study, we generated five NS3 mutants, some of which had significant impact on binding of small molecule inhibitors to the NS2B-NS3 interface and on viral protease activity[22]. We measured the binding affinity of **JMX0207** to these mutants as well. Our data showed that L58A abolished the binding of **JMX0207** (**Table 3**, **Figure 7D**). Two other mutations, I25A and H60A reduced the binding affinity 2 to 3 folds, whereas mutations Y23A and F46A do not have any effect.

Table 3. Binding affinity of JMX0207 to MBP-NS3 wild-type (WT) or mutant

	WT	Y23A	I25A	F46A	L58A	H60A
K_D (μM)	1.1	1.2	2.3	1.2	ND[a]	2.9

ND[a], no detectable binding.

Discussion

Dengue and Zika viruses cause significant human disease, for which there are no specific vaccines or therapies. Therefore, development of effective antivirals is urgent. Previously we identified an existing FDA-approved drug, niclosamide, as a potent antiviral against DENV and ZIKV. However, the poor pharmacokinetic properties of niclosamide prevent its clinical use to treat DENV and ZIKV infections.

In this study, we screened a small in-house compound library of niclosamide derivatives and identified **JMX0207** as a candidate inhibitor with improved properties. **JMX0207** inhibited the viral NS2B-NS3 protease activity of DENV2 with better efficacy *in vitro* than niclosamide. In cell culture, **JMX0207** significantly inhibited the growth of representative flaviviruses, including DENV2 and ZIKV, with EC_{50} in nanomolar range. By using IFA, WB, and qRT-PCR analyses, we showed that **JMX0207** also significantly inhibited viral RNA synthesis and protein production. More importantly, compared to niclosamide, **JMX0207** has reduced cytotoxicity profile towards

human cells, indicating a larger therapeutic window towards these flaviviruses. In addition, we showed that **JMX0207** could rescue ZIKV-relevant neural progenitor cells from viral infection in a dose-dependent manner. Moreover, **JMX0207** could almost completely protect 3D cortical organoids originated from neural stem cells from ZIKV infection. The findings establish the efficiency of **JMX0207** to eliminate infection of ZIKV from human neural progenitor cells, and provide a path forward to minimize the risk of fetal acquired microcephaly resulting from ZIKV infection of pregnant women.[54] Furthermore, we showed that **JMX0207** displayed significantly improved pharmacokinetic properties, compared to the parent compound niclosamide. The improved pharmacokinetics allowed us to carry out *in vivo* antiviral efficacy studies using an animal model for ZIKV infection. Our data showed that **JMX0207** treatment markedly reduced viral viremia in the A129 ZIKV mouse model infected with clinical strain ZIKV PRVABC59. Mechanistically, we showed that **JMX0207** directly binds to the viral NS3 protease with improved binding affinity, compared to its lead drug niclosamide. We also showed that JMX0207 treatment led to dose-dependent inhibition of viral polyprotein precursor processing, a direct consequence of inhibition of viral protease activity.

Conclusion

We conclude that the niclosamide derivative **JMX0207** is a valuable candidate for further study, due to its demonstrated ability to inhibit several activities required for ZIKV propagation. When paired with its reduced cytotoxicity profile and superior pharmacokinetic properties, these positive attributes indicate that **JMX0207** might effectively be used to combat viral progression following initial infection with ZIKV. Successful development of this compound would be a valuable tool in the prevention of negative ZIKV-related outcomes, including Guillain-Barre

syndrome, neuropathy and myelitis, as well as pregnancy-related outcomes including miscarriage, preterm birth, and congenital Zika syndrome.

Methods

Synthesis of niclosamide derivatives.

The synthetic route of compound **JMX0207** was described as below (**Scheme 1**), and the synthesis of other niclosamide derivatives was reported in our previous publications.[34-36, 38] The structures and purity of all synthesized compounds were confirmed by 1H and 13C NMR, HRMS and HPLC analysis, and all biologically evaluated compounds are >95% pure.

JMX0207 Synthesis.

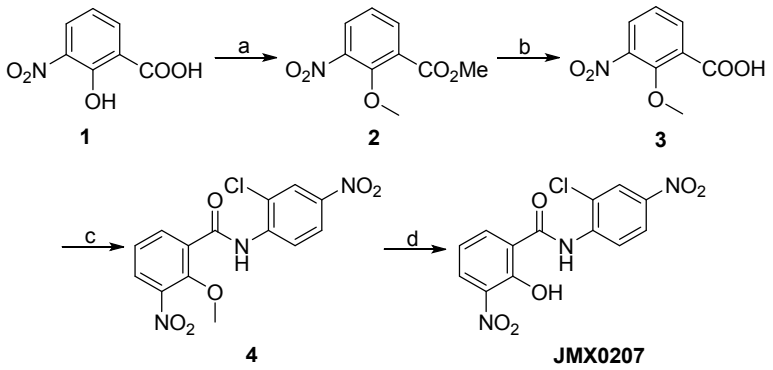

Scheme 1. JMX0207 synthesis route.

Reagents and conditions: (a) CH_3I, K_2CO_3, DMF, 50 °C, 24 h, 95%. (b) NaOH, H_2O/MeOH, r.t., 1 h, 93%. (c) 2-chloro-4-nitroaniline, $POCl_3$, pyridine, DCM, 0 °C to r.t., 8 h, 67%. (d) BBr_3, DCM, 0 °C to r.t., 12 h, 96%.

Methyl 2-methoxy-3-nitrobenzoate (2).

CH_3I (3.9 g, 27.3 mmol) was added to a solution of 3-nitrosalicylic acid (1.0 g, 5.5 mmol) and K_2CO_3 (2.3 g, 16.4 mmol) in 20 mL of DMF. The mixture was stirred at 50 °C for 24 hrs and then diluted with 300 mL of AcOEt. The resulting mixture was washed with water (3 × 70 mL) and

brine (50 mL), dried over Na_2SO_4, and concentrated *in vacuo*. The residue was purified by silica gel column (Hexane/EtOAc = 2/1) to afford compound **2** (1.1 g, 95%) as a yellow oil. ^{1}H NMR (300 MHz, $CDCl_3$) δ 8.01 – 7.89 (m, 1H), 7.85 – 7.78 (m, 1H), 7.23 – 7.09 (m, 1H), 3.91 (s, 3H), 3.87 (s, 3H). ^{13}C NMR (75 MHz, $CDCl_3$) δ 164.6, 153.1, 145.4, 135.5, 128.3, 127.2, 123.7, 64.1, 52.6.

2-Methoxy-3-nitrobenzoic acid (3).

NaOH (1.1 g, 27.3 mmol, in 6 mL of H_2O) was added to a solution of compound **2** (1.1 g, 5.5 mmol) in 10 mL of MeOH. The mixture was stirred at r.t. for 1 h, and then the pH value was adjusted to 5~6 with 1 M HCl (aq.). The mixture was extracted with EtOAc (2 × 120 mL) and washed with water (80 mL) and brine (60 mL), dried over Na_2SO_4, and concentrated to give acid **3** (1.0 g, 93%) as a light yellow solid for direct use in the next step.

***N*-(2-Chloro-4-nitrophenyl)-2-methoxy-3-nitrobenzamide (4).**

$POCl_3$ (3.9 g, 25.4 mmol) was added slowly at 0 °C to a solution of compound **3** (1.0 g, 5.1 mmol), 2-chloro-4-nitroaniline (876 mg, 5.1 mmol) and pyridine (8.0 g, 101.4 mmol) in 50 mL of DCM. After addition, the mixture was stirred at r.t. for 8 h and then poured into 200 mL of ice-water. Compound **4** (1.2 g, 67%) was isolated by filtration as a yellow solid. ^{1}H NMR (300 MHz, $CDCl_3$) δ 10.58 (s, 1H), 8.93 (d, J = 9.3 Hz, 1H), 8.46 (dd, J = 7.8, 1.8 Hz, 1H), 8.37 (d, J = 2.7 Hz, 1H), 8.24 (dd, J = 9.3, 2.4 Hz, 1H), 8.06 (dd, J = 8.1, 1.8 Hz, 1H), 7.46 (t, J = 8.1 Hz, 1H), 4.12 (s, 3H).^{13}C NMR (75 MHz, $CDCl_3$) δ 161.9, 151.7, 144.4, 143.6, 140.7, 137.0, 129.9, 128.2, 125.3, 125.1, 123.8, 123.1, 121.1, 64.9.

***N*-(2-Chloro-4-nitrophenyl)-2-hydroxy-3-nitrobenzamide (JMX0207).**

BBr_3 (7.4 ml, 7.40 mmol, 1M in DCM) was added dropwise at 0 °C to a solution of compound **4** (1.3 g, 3.70 mmol) in 250 mL of DCM. The mixture was stirred at r.t. for 2 h. Then the mixture

was poured into 200 mL of ice water. The yellow precipitate **JMX0207** was isolated by filtration. The organic layer was separated and concentrated. Then 50 mL of MeOH was added and the mixture was stirred at r.t for 20 min. The yellow solid was isolated by filtration. The two parts of yellow solids were combined to afford 1.2 g (96%) of compound **JMX0207** in total. HPLC purity 99.9% (t_R = 18.75 min). ^{1}H NMR (300 MHz, DMSO-d_6) δ 12.10 (s, 1H), 8.65 (d, J = 9.3 Hz, 1H), 8.42 (d, J = 2.4 Hz, 1H), 8.34 – 8.24 (m, 2H), 8.13 (d, J = 8.1 Hz, 1H), 7.03 (t, J = 7.8 Hz, 1H). ^{13}C NMR (75 MHz, DMSO-d_6) δ 164.2, 154.1, 143.1, 141.3, 139.1, 136.3, 129.8, 124.8, 124.1, 123.6, 122.5, 122.4, 117.3. HRMS (ESI) calcd for $C_{13}H_9ClN_3O_6$ 338.0180 $(M + H)^+$, found 338.0172.

Cloning, Expression and Purification.

All clones and proteins were generated as previously described.[21-22]

Split Luciferase Complementation (SLC) Assay.

The SLC assay was performed as previously described.[21-22, 55]

Protease Inhibition Assay.

The protease inhibition assay was performed using the refolded DENV2 NS3 fusion protein (50 nM) and a fluorescence resonance energy transfer (FRET) peptide substrate (100 μM) (Abz-RRRRSAG-nTyr (NeoBiolab)), as described previously.[21-23, 55] Substrate cleavage was monitored at excitation/emission wavelengths of 360 nm/420 nm (Abz substrate) by a BioTek Flx800. The rate of increase in relative fluorescence unit (RFU) over time was calculated in the linear range and normalized as a percent of the DMSO control. The $IC_{50}/CC_{50}/EC_{50}$ was determined by fitting the dose-responsive curve with a non-linear regression function using the GraphPad Prism 8 (San Diego, CA). All experiments were performed in triplicates.

Cytotoxicity Assay.

Cytotoxicity was measured by a WST-8 cell proliferation assay kit (Dojindo Molecular Technologies, Inc.) as previously described.[21] All experiments were performed in triplicates.

Viral Titer Reduction Assay.

A viral titer reduction assay was used to determine the compounds' effect on DENV2 and ZIKV strains, as described previously[21-22]. Human A549 lung carcinoma cells and human primary neural progenitor cells were used, as described previously.[21-22] All experiments were performed in triplicates.

Immunofluorescence Assay.

The immunofluorescence assay was performed using ZIKV-infected cells treated with DMSO or **JMX0207**, as described previously.[21-22] A mouse monoclonal pan anti-E antibody 4G2 (ATCC) and a DyLight® 488 goat anti-mouse IgG (ImmunoReagents, Inc.) were used to monitor viral E protein expression, as described previously.[21-22]

Quantitative qRT-PCR.

Quantitative qRT-PCR was performed as described previously.[21-22] ZIKV primers CCGCTGCCCAACACAAG and CCACTAAYGTTCTTTTGCAGACAT with ZIKV probe Cy5-AGCCTACCT/TAO/TGACAAGCAGTCAGACACTCAA-IAbRQSp were used. The 2−ΔΔCT ("delta-delta Ct") method was used to quantify samples. All experiments were performed in triplicates.

Western Blot.

Western blot was performed using anti-ZIKV NS3 (GTX133309, GeneTex, Inc.) and anti-GAPDH (CB1001, EMD Millipore) antibodies, as described previously.[21, 23] All experiments were performed in triplicates.

DENV2 Replicon Assay.

BHK-21 cells stably expressing DENV2 replicon with a *Renilla luciferase* (*Rluc*) reporter gene[53] were seeded into white 96-well plate at a density of 2 x 10^5 cells per well. The cells were incubated at 37°C in a humidified incubator with 5% CO_2 for hrs in a 100 µl medium containing Minimal Essential Medium (MEM) supplemented with 10% fetal bovine serum (FBS), 100 I.U./ml penicillin, 100 µg/ml streptomycin, and 300 µg/ml G418. Upon 24 hrs incubation, culture medium was discarded. Fresh culture medium of 100 µl with a concentration series of compounds or DMSO control was added to the cells in triplicates. The culture was further incubated for 48 hours. The cells were then washed twice with 100 µl phosphate-buffered saline (PBS), followed by addition of 25 µl of a lysis buffer containing 1X PBS and 1% Triton X-100. The mixture was incubated at room temperature with gentle shaking (50 rpm) for 30 minutes. Assay buffer (125 µl) containing 1X PBS, 0.05% (3-((3-cholamidopropyl) dimethylammonio)-1-propanesulfonate)(CHAPS), and 0.1% BSA was then added to each well. In the meantime, a fresh 4X working substrate coelenterazine was prepared by diluting 1 µl of stock coelenterazine (2.4 mM) dissolved in ethanol into 10 ml assay buffer (10,000-fold dilution). Finally, 50 µl 4X substrate coelenterazine was added to each well with a final substrate concentration of 0.06 µM, using a Veritas luminometer. The luminescence was recorded immediately using the Veritas luminometer. The luminescence data was normalized to DMSO control. The EC_{50} was determined by nonlinear regression fitting of normalized experimental data in GraphPad Prism 8.0 (San Diego, CA). All experiments were performed in triplicates.

Docking.

The crystal structure of NS3pro of DENV2 (PDB Code: 2FOM) was downloaded from RCSB PDB bank. After excluding the cofactor NS2B peptide, the structure was preprocessed and optimized with Schrödinger Protein Preparation Wizard using default settings. The 3D structure

of JMX0207 and niclosamide were created using Schrödinger Maestro and prepared with LigPrep to generate a low energy conformation suitable for docking. The Induced Fit Docking (IFD) protocol of Schrödinger Small-Molecule Drug Discovery Suite was employed in this docking study. The grid box for docking was centered on the 2B53 binding site. The box size was set to 20 Å on each side. Selected side chains of R24, K26, and M59 were temporarily trimmed (the equivalent of being mutated to alanine) during the initial IFD process and were restored later. The receptor-ligand complexes structures generated from IFD docking were imported into Schrödinger Maestro for visualization and analysis of binding site interactions.

Surface Plasmon Resonance.

Surface plasmon resonance (SPR) was used to determine the affinity and kinetic analyses of the interactions between JMX0207 and the MBP-NS3 proteins at 25 °C using a ProteOn XPR36 SPR instrument (Bio-Rad). The MBP-NS3 wild-type or mutant proteins were immobilized onto a ProteOn™ GLH sensor chip (~9,000 RU) (Bio-Rad). A 2-fold dilution series of compounds were injected as the analytes. A blank surface blocked by ethanolamine was used as the control surface. The experiment was carried out at a flow rate of 100 µl/min using a PBSTD buffer containing 1x PBS, 0.005% surfactant P20, and 5% DMSO. Association (k_a) and dissociation (k_d) rates, as well as the dissociation constant (K_D), were obtained by global fitting of the SPR data from multiple concentrations to a simple 1:1 Langmuir binding model, using the ProteOn Manager software suite (Bio-Rad).

Culturing of human iPSCs.

Human iPSC F11350.1 culture was maintained in feed-free conditions using mTeSR1 medium (StemCell Technologies #85851) with 5X supplement (StemCell Technologies #85852).

Cells were maintained on six-well plates coated with human embryonic stem cell-qualified Matrigel at a 1:60 dilution (Corning Catalog #354277) and passaged with ReLeSR (StemCell Technologies #05872). Cortical 3D organoids were generated based on the protocol described by Yoon *et al*.[50] Briefly, iPSCs were dissociated with accutase (ThermoFisher #A1110501) and then plated at a density of $3x10^6$ cells per well in AggreWell 800 24-well plate (StemCell Technologies #34811) in Essential 8™ medium (ThermoFisher #A1517001) supplemented with 10μM rock inhibitor (Tocris #Y27632). The plate was centrifuged at 100 x g for 3 min and incubated at 37°C overnight. The next day (culture day 0) the organoids were transferred to a low attachment 10cm plate (Corning #3262) and maintained in 10mL of neural induction medium (Essential 6™ medium, Life Technologies, #A1516401) supplemented with two SMAD pathway inhibitors, 10 μM SB431541 (R&D #1614/50) and 2.5 μM dorsomorphin (Tocris #3093), and Wnt pathway inhibitor 2.5 μM XAV-939 (Tocris #XAV-939). Media were exchanged daily. On day 6, the medium was changed to neural expansion medium (Neuralbasal A medium, ThermoFisher #10888) supplemented with 2% B27 (without Vit A; ThermoFisher #12587001), 1% antibiotic-antimycotic (ThermoFisher #15240062), 1% glutaMAX (ThermoFisher # 35050061), 20 ng/mL FGF2 (R&D #233-FB-500) and 20 ng/mL EGF2 (PeproTech #AF-100-15). Media were exchanged daily.

Cryopreservation.

Organoids were fixed in 4% paraformaldehyde (Santa Cruz) overnight at 4°C. They were then washed three times in PBS and transferred to 30% sucrose solution for 72 h. Organoids were then transferred into plastic cryomold (10 X 10 X 5mm; Tissue Tek cat. no. 4565) with embedding medium (Tissue-Tek OCT compound, Sakura Finetek 4583) and stored at −80°C. For

immunohistochemistry, 20 μm thick sections were cut with a Leica cryostat (model CM3050S).

Immunohistochemistry.

Cryosections were blocked in 3% bovine serum albumin (BSA), 10% normal goat serum (NGS), and 0.3% Triton X–100 diluted in PBS for 1 hour at room temperature. The sections were incubated overnight at 4°C with primary antibodies diluted in blocking solution. Sections were washed three times with PBS and then incubated with appropriate secondary antibodies diluted in blocking solution for 1 hour. The following primary antibodies were used for immunohistochemistry: anti-Pax-6 (1:200; Biolegend #901301), anti-Sox2 (1:100; Santa Cruz #sc-365823), anti-FoxG1 (1:500; Takara #M227), Sox10 (1: 100; Santa Cruz # sc369692), and anti-tubulin III (1:1000; Sigma #T8660).

Pharmacokinetics.

Two- to three-month-old female B6 mice were used for the study. Four to five mice per group were given niclosamide at 40 mg/kg (in 1% DMSO and 0.5% carboxymethylcellulose) or JMX0207 in the same vehicle at the indicated dose by oral gavage. Sample preparation and liquid chromatography with tandem mass spectrometry (LC-MS/MS) detection of niclosamide and JMX0207 were essentially the same as described in a previous study and were performed using a Sciex 4000 Q-Trap mass spectrometer (AB SCIEX, Framingham, MA) with the Agilent 1200 high-performance liquid chromatography system (Agilent Technologies, Santa Clara, CA).[29] JMX0207 was monitored at m/z 336/171. Declustering potential, entrance potential, collision energy, and collision cell exit potential were optimized for detection and quantification of JMX0207 at -45, -10, -35, and -14V, respectively. Data from 4 or 5 mice at each time point were averaged and used to calculate pharmacokinetic parameters, using a pharmacokinetic solver (Microsoft, Redmond, WA) by assuming a noncompartmental model. Statistical significance of

various data comparisons was determined with the use of GraphPad Prism (GraphPad Software, La Jolla, CA). Student's t-test was used. P values < 0.05 were considered statistically significant.

***In vivo* protection efficacy.**

All animal studies involving infectious ZIKV were conducted at an Animal Biosafety Level 2 (ABSL-2) facility at the Wadsworth Center with Institutional Biosafety and Animal Welfare Committee approval. The *in vivo* antiviral activity of **JMX0207** was evaluated in a viremia animal model.

A group of four-week-old A129 mice were infected by subcutaneous injection with 1.7×10^5 PFU of the PRVABC59 strain. Then, the infected mice were administered **JMX0207** at 20 mg/kg of body weight (n=10) or with vehicle control (n=10) every day for 3 consecutive days post-infection (dpi). Mice were observed daily for signs of illness and mortality. Viremia on day 3 post-infection (pi) was determined by plaque forming assay, and statistical analysis was performed using the unpaired, two-tailed t-test (Prism).

AUTHOR INFORMATION

Corresponding Authors

Jia Zhou -- Chemical Biology Program, Department of Pharmacology and Toxicology, University of Texas Medical Branch, Galveston, TX 77555, USA; Email: jizhou@utmb.edu

Hongmin Li -- Wadsworth Center, New York State Department of Health, 120 New Scotland Ave, Albany, NY 12208, USA; Department of Biomedical Sciences, School of Public Health, University at Albany, Albany, NY 12201, USA; Email: Hongmin.li@health.ny.gov

Other Authors

Zhong Li -- Wadsworth Center, New York State Department of Health, 120 New Scotland Ave, Albany, NY 12208, USA; Email: Zhong.li@health.ny.gov

Jimin Xu -- Chemical Biology Program, Department of Pharmacology and Toxicology, University of Texas Medical Branch, Galveston, TX 77555, USA; Email: jimxu@utmb.edu

Yuekun Lang -- Wadsworth Center, New York State Department of Health, 120 New Scotland Ave, Albany, NY 12208, USA; Email: yuekun.lang@health.ny.gov

Xiaoyu Fan -- Department of Pharmacology and Toxicology, College of Pharmacy, University of Arizona, Tucson, AZ 85721, USA; Email: xfan@pharmacy.arizona.edu

Lili Kuo -- Wadsworth Center, New York State Department of Health, 120 New Scotland Ave, Albany, NY 12208, USA; Email: lili.kuo@health.ny.gov

Lianna D'Brant -- The Neural Stem Cell Institute, 1 Discovery Drive, Rensselaer, NY 12144, USA; Email: liannadbrant@neuralsci.org

Subodh Kumar Samrat --Wadsworth Center, New York State Department of Health, 120 New Scotland Ave, Albany, NY 12208, USA; Email: subodh.samrat@health.ny.gov

Nicole Trudeau -- The Neural Stem Cell Institute, 1 Discovery Drive, Rensselaer, NY 12144, USA; Email: nicoletrudeau@neuralsci.org

Anil M. Tharappel -- Wadsworth Center, New York State Department of Health, 120 New Scotland Ave, Albany, NY 12208, USA; Email: anil.tharappel@health.ny.gov

Natasha Rugenstein -- The Neural Stem Cell Institute, 1 Discovery Drive, Rensselaer, NY 12144, USA; Email: Natasharugenstein@neuralsci.org

Cheri A Koetzner -- Wadsworth Center, New York State Department of Health, 120 New Scotland Ave, Albany, NY 12208, USA; Email: cheri.koetzner@health.ny.gov

Saiyang Hu -- Wadsworth Center, New York State Department of Health, 120 New Scotland Ave, Albany, NY 12208, USA; Email: saiyang.hu@health.ny.gov

Jing Zhang -- Wadsworth Center, New York State Department of Health, 120 New Scotland Ave, Albany, NY 12208, USA; Email: jingzhang537@gmail.com

Haiying Chen -- Chemical Biology Program, Department of Pharmacology and Toxicology, University of Texas Medical Branch, Galveston, TX 77555, USA; Email: haichen@UTMB.EDU

Laura D Kramer --Wadsworth Center, New York State Department of Health, 120 New Scotland Ave, Albany, NY 12208, USA**;** Department of Biomedical Sciences, School of Public Health, University at Albany, Albany, NY 12201, USA; Email: laura.kramer@health.ny.gov

David Butler -- The Neural Stem Cell Institute, 1 Discovery Drive, Rensselaer, NY 12144, USA; Email: davidbutler@neuralsci.org

Qing-Yu Zhang -- Department of Pharmacology and Toxicology, College of Pharmacy, University of Arizona, Tucson, AZ 85721, USA; Email: qyzhang@pharmacy.arizona.edu

Author Contributions

[#]Z.L. and J.X. contributed equally to this work.

Notes

The authors declare no competing financial interests.

Acknowledgments

We thank Dr. Padmanabhan at Georgetown University for the gift of the DENV2 replicon BHK-21 cell line. We thank the Wadsworth Center Tissue Culture Core facility for help with cell cultures and media preparation, the Biochemistry Core for SPR assistance, the animal facility for animal care, the Advanced Light Microscopy Core for immunofluorescence/confocal imaging assistance, and Dr. McClive-Reed of Heath Research, Inc. for helpful suggestions. Dr. Jia Zhou is also supported by the John D. Stobo, M.D. Distinguished Chair Endowment Fund. This work was partially supported by NIH grants AI131669, AI133219, AI140491, and AI134568.

ABBREVIATIONS

ABSL-2, Animal Biosafety Level 2; BSA, bovine serum albumin; CHAPS ((3-((3-cholamidopropyl) dimethylammonio)-1-propanesulfonate)); DENV, dengue virus; DMSO, dimethyl sulfoxide; DN2, dengue virus serotype 2; dpi, days post-infection; FBS, fetal bovine serum; FRET, fluorescence resonance energy transfer; HNPC, human neural progenitor cells; IFA, immunofluorescence assay; iPCS, induced pluripotent stem cell; LC-MS/MS, liquid chromatography with tandem mass spectrometry; MEM, Minimum Essential Medium; MOI, multiplicity of infection; NGS, normal goat serum; PBS, phosphate-buffered saline; PFU, plaque forming unit; PTSA, protein thermal shift assay; qRT-PCR, quantitative reverse transcription polymerase chain reaction; RFU, relative fluorescence unit; RLU, relative luminescence unit; SLC, split luciferase complementation; SPR, surface plasmon resonance; WB, Western blot; ZIKV/ZK, Zika virus

REFERENCES

1. Calvet, G.; Aguiar, R. S.; Melo, A. S.; Sampaio, S. A.; de Filippis, I.; Fabri, A.; Araujo, E. S.; de Sequeira, P. C.; de Mendonca, M. C.; de Oliveira, L.; Tschoeke, D. A.; Schrago, C. G.; Thompson, F. L.; Brasil, P.; Dos Santos, F. B.; Nogueira, R. M.; Tanuri, A.; de Filippis, A. M., Detection and sequencing of Zika virus from amniotic fluid of fetuses with microcephaly in Brazil: a case study. *Lancet Infect Dis* **2016,** *16*, 653-60. DOI: S1473-3099(16)00095-5 [pii] 10.1016/S1473-3099(16)00095-5.

2. Thomas, D. L.; Sharp, T. M.; Torres, J.; Armstrong, P. A.; Munoz-Jordan, J.; Ryff, K. R.; Martinez-Quinones, A.; Arias-Berrios, J.; Mayshack, M.; Garayalde, G. J.; Saavedra, S.; Luciano, C. A.; Valencia-Prado, M.; Waterman, S.; Rivera-Garcia, B., Local Transmission of Zika Virus - Puerto Rico, November 23, 2015-January 28, 2016. *MMWR Morb Mortal Wkly Rep* **2016,** *65* (6), 154-8. DOI: 10.15585/mmwr.mm6506e2.

3. Martines, R. B.; Bhatnagar, J.; Keating, M. K.; Silva-Flannery, L.; Muehlenbachs, A.; Gary, J.; Goldsmith, C.; Hale, G.; Ritter, J.; Rollin, D.; Shieh, W. J.; Luz, K. G.; Ramos, A. M.; Davi, H. P.; Kleber de Oliveria, W.; Lanciotti, R.; Lambert, A.; Zaki, S., Notes from the Field: Evidence of Zika Virus Infection in Brain and Placental Tissues from Two Congenitally Infected Newborns and Two Fetal Losses - Brazil, 2015. *MMWR Morb Mortal Wkly Rep* **2016,** *65* (6), 159-60. DOI: 10.15585/mmwr.mm6506e1.

4. Rodriguez-Morales, A. J., Zika and microcephaly in Latin America: An emerging threat for pregnant travelers? *Travel Med Infect Dis* **2016,** *14*, 5-6. DOI: S1477-8939(16)00013-2 [pii] 10.1016/j.tmaid.2016.01.011.

5. Li, C.; Xu, D.; Ye, Q.; Hong, S.; Jiang, Y.; Liu, X.; Zhang, N.; Shi, L.; Qin, C. F.; Xu, Z., Zika Virus Disrupts Neural Progenitor Development and Leads to Microcephaly in Mice. *Cell Stem Cell* **2016**. DOI: S1934-5909(16)30084-4 [pii] 10.1016/j.stem.2016.04.017.

6. Patino-Barbosa, A. M.; Medina, I.; Gil-Restrepo, A. F.; Rodriguez-Morales, A. J., Zika: another sexually transmitted infection? *Sex Transm Infect* **2015,** *91* (5), 359. DOI: 10.1136/sextrans-2015-052189 sextrans-2015-052189 [pii].

7. Musso, D.; Roche, C.; Robin, E.; Nhan, T.; Teissier, A.; Cao-Lormeau, V. M., Potential sexual transmission of Zika virus. *Emerg Infect Dis* **2015,** *21* (2), 359-61. DOI: 10.3201/eid2102.141363.

8. Musso, D.; Nhan, T.; Robin, E.; Roche, C.; Bierlaire, D.; Zisou, K.; Shan Yan, A.; Cao-Lormeau, V. M.; Broult, J., Potential for Zika virus transmission through blood transfusion demonstrated during an outbreak in French Polynesia, November 2013 to February 2014. *Euro Surveill* **2014,** *19* (14). DOI: 20761 [pii].

9. Foy, B. D.; Kobylinski, K. C.; Chilson Foy, J. L.; Blitvich, B. J.; Travassos da Rosa, A.; Haddow, A. D.; Lanciotti, R. S.; Tesh, R. B., Probable non-vector-borne transmission of Zika virus, Colorado, USA. *Emerg Infect Dis* **2011,** *17* (5), 880-2. DOI: 10.3201/eid1705.101939.

10. Duggal, N. K.; Ritter, J. M.; Pestorius, S. E.; Zaki, S. R.; Davis, B. S.; Chang, G. J.; Bowen, R. A.; Brault, A. C., Frequent Zika Virus Sexual Transmission and Prolonged Viral RNA Shedding in an Immunodeficient Mouse Model. *Cell Rep* **2017,** *18* (7), 1751-1760. DOI: S2211-1247(17)30113-4 [pii] 10.1016/j.celrep.2017.01.056.

11. Hirsch, A. J.; Smith, J. L.; Haese, N. N.; Broeckel, R. M.; Parkins, C. J.; Kreklywich, C.; DeFilippis, V. R.; Denton, M.; Smith, P. P.; Messer, W. B.; Colgin, L. M.; Ducore, R. M.; Grigsby, P. L.; Hennebold, J. D.; Swanson, T.; Legasse, A. W.; Axthelm, M. K.; MacAllister, R.; Wiley, C.

A.; Nelson, J. A.; Streblow, D. N., Zika Virus infection of rhesus macaques leads to viral persistence in multiple tissues. *PLoS Pathog* **2017,** *13* (3), e1006219. DOI: 10.1371/journal.ppat.1006219 PPATHOGENS-D-16-02436 [pii].

12. Govero, J.; Esakky, P.; Scheaffer, S. M.; Fernandez, E.; Drury, A.; Platt, D. J.; Gorman, M. J.; Richner, J. M.; Caine, E. A.; Salazar, V.; Moley, K. H.; Diamond, M. S., Zika virus infection damages the testes in mice. *Nature* **2016,** *540* (7633), 438-442. DOI: 10.1038/nature20556 nature20556 [pii].

13. Aguiar, M.; Stollenwerk, N.; Halstead, S. B., The Impact of the Newly Licensed Dengue Vaccine in Endemic Countries. *PLoS Negl Trop Dis* **2016,** *10* (12), e0005179. DOI: 10.1371/journal.pntd.0005179 PNTD-D-16-00650 [pii].

14. Brecher, M.; Zhang, J.; Li, H., The flavivirus protease as a target for drug discovery. *Virol Sin* **2013,** *28* (6), 326-36. DOI: 10.1007/s12250-013-3390-x.

15. Lindenbach, B.; Rice, C. M., *Flaviviridae: The virus and Their Replication,*. Fourth ed.; Lippincott William & Wilkins: 2001.

16. Liu, L.; Dong, H.; Chen, H.; Zhang, J.; Ling, H.; Li, Z.; Shi, P. Y.; Li, H., Flavivirus RNA cap methyltransferase: structure, function, and inhibition. *Front Biol* **2010,** *5* (4), 286-303.

17. Kang, C.; Keller, T. H.; Luo, D., Zika Virus Protease: An Antiviral Drug Target. *Trends Microbiol* **2017,** *25* (10), 797-808. DOI: S0966-842X(17)30171-3 [pii] 10.1016/j.tim.2017.07.001.

18. Nitsche, C., Proteases from dengue, West Nile and Zika viruses as drug targets. *Biophys Rev* **2019,** *11* (2), 157-165. DOI: 10.1007/s12551-019-00508-3 10.1007/s12551-019-00508-3 [pii].

19. Noble, C. G.; Chen, Y. L.; Dong, H.; Gu, F.; Lim, S. P.; Schul, W.; Wang, Q. Y.; Shi, P. Y., Strategies for development of Dengue virus inhibitors. *Antiviral research* **2010,** *85* (3), 450-62. DOI: 10.1016/j.antiviral.2009.12.011.

20. Yuan, S.; Chan, J. F.; den-Haan, H.; Chik, K. K.; Zhang, A. J.; Chan, C. C.; Poon, V. K.; Yip, C. C.; Mak, W. W.; Zhu, Z.; Zou, Z.; Tee, K. M.; Cai, J. P.; Chan, K. H.; de la Pena, J.; Perez-Sanchez, H.; Ceron-Carrasco, J. P.; Yuen, K. Y., Structure-based discovery of clinically approved drugs as Zika virus NS2B-NS3 protease inhibitors that potently inhibit Zika virus infection in vitro and in vivo. *Antiviral Res* **2017,** *145*, 33-43. DOI: S0166-3542(17)30175-4 [pii] 10.1016/j.antiviral.2017.07.007.

21. Li, Z.; Brecher, M.; Zhang, J.; Sakamuru, S.; Liu, B.; Huang, R.; Koetzner, C. A.; Allen, C. A.; Jones, S. A.; Deng, Y. Q.; Chen, H.; Gao, F.; Qin, C. F.; Lin, Q.; Banavali, N.; Zhou, J.; Boles, N.; Xia, M. K., L.D.; Li, H. M., Existing drugs as broad-spectrum and potent inhibitors for Zika virus by targeting NS2B-NS3 interaction. *Cell Res* **2017,** *27*, 1046-64.

22. Li, Z.; Sakamuru, S.; Huang, R.; Brecher, M.; Koetzner, C. A.; Zhang, J.; Chen, H.; Qin, C. F.; Zhang, Q. Y.; Zhou, J.; Kramer, L. D.; Xia, M.; Li, H., Erythrosin B is a potent and broad-spectrum orthosteric inhibitor of the flavivirus NS2B-NS3 protease. *Antiviral Res* **2018,** *150*, 217-225. DOI: S0166-3542(17)30450-3 [pii] 10.1016/j.antiviral.2017.12.018.

23. Brecher, M.; Li, Z.; Liu, B.; Zhang, J.; Koetzner, C. A.; Alifarag, A.; Jones, S. A.; Lin, Q.; Kramer, L. D.; Li, H., A conformational switch high-throughput screening assay and allosteric inhibition of the flavivirus NS2B-NS3 protease. *PLoS Pathog* **2017,** *13* (5), e1006411. DOI: 10.1371/journal.ppat.1006411 PPATHOGENS-D-16-02684 [pii].

24. Yao, Y.; Huo, T.; Lin, Y. L.; Nie, S.; Wu, F.; Hua, Y.; Wu, J.; Kneubehl, A. R.; Vogt, M. B.; Rico-Hesse, R.; Song, Y., Discovery, X-ray Crystallography and Antiviral Activity of

Allosteric Inhibitors of Flavivirus NS2B-NS3 Protease. *J Am Chem Soc* **2019,** *141* (17), 6832-6836. DOI: 10.1021/jacs.9b02505.

25. Shiryaev, S. A.; Farhy, C.; Pinto, A.; Huang, C. T.; Simonetti, N.; Elong Ngono, A.; Dewing, A.; Shresta, S.; Pinkerton, A. B.; Cieplak, P.; Strongin, A. Y.; Terskikh, A. V., Characterization of the Zika virus two-component NS2B-NS3 protease and structure-assisted identification of allosteric small-molecule antagonists. *Antiviral Res* **2017,** *143*, 218-229. DOI: S0166-3542(17)30154-7 [pii] 10.1016/j.antiviral.2017.04.015.

26. Mazzon, M.; Ortega-Prieto, A. M.; Imrie, D.; Luft, C.; Hess, L.; Czieso, S.; Grove, J.; Skelton, J. K.; Farleigh, L.; Bugert, J. J.; Wright, E.; Temperton, N.; Angell, R.; Oxenford, S.; Jacobs, M.; Ketteler, R.; Dorner, M.; Marsh, M., Identification of Broad-Spectrum Antiviral Compounds by Targeting Viral Entry. *Viruses* **2019,** *11* (2). DOI: E176 [pii] 10.3390/v11020176 v11020176 [pii].

27. Kao, J. C.; HuangFu, W. C.; Tsai, T. T.; Ho, M. R.; Jhan, M. K.; Shen, T. J.; Tseng, P. C.; Wang, Y. T.; Lin, C. F., The antiparasitic drug niclosamide inhibits dengue virus infection by interfering with endosomal acidification independent of mTOR. *PLoS Negl Trop Dis* **2018,** *12* (8), e0006715. DOI: 10.1371/journal.pntd.0006715 PNTD-D-18-00285 [pii].

28. Xu, J.; Shi, P. Y.; Li, H.; Zhou, J., Broad Spectrum Antiviral Agent Niclosamide and Its Therapeutic Potential. *ACS Infect Dis* **2020**. DOI: 10.1021/acsinfecdis.0c00052.

29. Fan, X.; Li, H.; Ding, X.; Zhang, Q. Y., Contributions of Hepatic and Intestinal Metabolism to the Disposition of Niclosamide, a Repurposed Drug with Poor Bioavailability. *Drug Metab Dispos* **2019,** *47* (7), 756-763. DOI: 10.1124/dmd.119.086678 dmd.119.086678 [pii].

30. Burock, S.; Daum, S.; Keilholz, U.; Neumann, K.; Walther, W.; Stein, U., Phase II trial to investigate the safety and efficacy of orally applied niclosamide in patients with metachronous or

sychronous metastases of a colorectal cancer progressing after therapy: the NIKOLO trial. *BMC Cancer* **2018,** *18* (1), 297. DOI: 10.1186/s12885-018-4197-9 10.1186/s12885-018-4197-9 [pii].

31. Barbosa, E. J.; Lobenberg, R.; de Araujo, G. L. B.; Bou-Chacra, N. A., Niclosamide repositioning for treating cancer: Challenges and nano-based drug delivery opportunities. *Eur J Pharm Biopharm* **2019,** *141*, 58-69. DOI: S0939-6411(19)30240-1 [pii] 10.1016/j.ejpb.2019.05.004.

32. Chen, W.; Mook, R. A., Jr.; Premont, R. T.; Wang, J., Niclosamide: Beyond an antihelminthic drug. *Cell Signal* **2018,** *41*, 89-96. DOI: S0898-6568(17)30101-8 [pii] 10.1016/j.cellsig.2017.04.001.

33. Fan, X.; Xu, J.; Files, M.; Cirillo, J. D.; Endsley, J. J.; Zhou, J.; Endsley, M. A., Dual activity of niclosamide to suppress replication of integrated HIV-1 and Mycobacterium tuberculosis (Beijing). *Tuberculosis (Edinb)* **2019,** *116S*, S28-S33. DOI: S1472-9792(19)30147-7 [pii] 10.1016/j.tube.2019.04.008.

34. Xu, J.; Pachon-Ibanez, M. E.; Cebrero-Cangueiro, T.; Chen, H.; Sanchez-Cespedes, J.; Zhou, J., Discovery of niclosamide and its O-alkylamino-tethered derivatives as potent antibacterial agents against carbapenemase-producing and/or colistin resistant Enterobacteriaceae isolates. *Bioorg Med Chem Lett* **2019,** *29* (11), 1399-1402. DOI: S0960-894X(19)30171-4 [pii] 10.1016/j.bmcl.2019.03.032.

35. Chen, H.; Yang, Z.; Ding, C.; Xiong, A.; Wild, C.; Wang, L.; Ye, N.; Cai, G.; Flores, R. M.; Ding, Y.; Shen, Q.; Zhou, J., Discovery of potent anticancer agent HJC0416, an orally bioavailable small molecule inhibitor of signal transducer and activator of transcription 3 (STAT3). *Eur J Med Chem* **2014,** *82*, 195-203. DOI: 10.1016/j.ejmech.2014.05.049 S0223-5234(14)00473-5 [pii].

36. Chen, H.; Yang, Z.; Ding, C.; Chu, L.; Zhang, Y.; Terry, K.; Liu, H.; Shen, Q.; Zhou, J., Discovery of O-Alkylamino Tethered Niclosamide Derivatives as Potent and Orally Bioavailable Anticancer Agents. *ACS Med Chem Lett* **2013,** *4* (2), 180-185. DOI: 10.1021/ml3003082.

37. Wang, Y.; Wang, S.; Wu, Y.; Ren, Y.; Li, Z.; Yao, X.; Zhang, C.; Ye, N.; Jing, C.; Dong, J.; Zhang, K.; Sun, S.; Zhao, M.; Guo, W.; Qu, X.; Qiao, Y.; Chen, H.; Kong, L.; Jin, R.; Wang, X.; Zhang, L.; Zhou, J.; Shen, Q.; Zhou, X., Suppression of the Growth and Invasion of Human Head and Neck Squamous Cell Carcinomas via Regulating STAT3 Signaling and the miR-21/beta-catenin Axis with HJC0152. *Mol Cancer Ther* **2017,** *16* (4), 578-590. DOI: 10.1158/1535-7163.MCT-16-0606 1535-7163.MCT-16-0606 [pii].

38. Chen, H.; Yang, Z.; Ding, C.; Chu, L.; Zhang, Y.; Terry, K.; Liu, H.; Shen, Q.; Zhou, J., Fragment-based drug design and identification of HJC0123, a novel orally bioavailable STAT3 inhibitor for cancer therapy. *Eur J Med Chem* **2013,** *62*, 498-507. DOI: 10.1016/j.ejmech.2013.01.023 S0223-5234(13)00051-2 [pii].

39. Thorne, N.; Shen, M.; Lea, W. A.; Simeonov, A.; Lovell, S.; Auld, D. S.; Inglese, J., Firefly luciferase in chemical biology: a compendium of inhibitors, mechanistic evaluation of chemotypes, and suggested use as a reporter. *Chem Biol* **2012,** *19* (8), 1060-72. DOI: 10.1016/j.chembiol.2012.07.015 S1074-5521(12)00268-2 [pii].

40. Vernekar, S. K.; Qiu, L.; Zhang, J.; Kankanala, J.; Li, H.; Geraghty, R. J.; Wang, Z., 5'-Silylated 3'-1,2,3-triazolyl Thymidine Analogues as Inhibitors of West Nile Virus and Dengue Virus. *J Med Chem* **2015,** *58* (9), 4016-28. DOI: 10.1021/acs.jmedchem.5b00327.

41. Chambers, S. M.; Fasano, C. A.; Papapetrou, E. P.; Tomishima, M.; Sadelain, M.; Studer, L., Highly efficient neural conversion of human ES and iPS cells by dual inhibition of SMAD signaling. *Nat Biotechnol* **2009,** *27* (3), 275-80. DOI: 10.1038/nbt.1529 nbt.1529 [pii].

42. Tabata, T.; Petitt, M.; Puerta-Guardo, H.; Michlmayr, D.; Wang, C.; Fang-Hoover, J.; Harris, E.; Pereira, L., Zika Virus Targets Different Primary Human Placental Cells, Suggesting Two Routes for Vertical Transmission. *Cell Host Microbe* **2016,** *20* (2), 155-66. DOI: 10.1016/j.chom.2016.07.002 S1931-3128(16)30300-6 [pii].

43. Tang, H.; Hammack, C.; Ogden, S. C.; Wen, Z.; Qian, X.; Li, Y.; Yao, B.; Shin, J.; Zhang, F.; Lee, E. M.; Christian, K. M.; Didier, R. A.; Jin, P.; Song, H.; Ming, G. L., Zika Virus Infects Human Cortical Neural Progenitors and Attenuates Their Growth. *Cell Stem Cell* **2016,** *18* (5), 587-90. DOI: 10.1016/j.stem.2016.02.016 S1934-5909(16)00106-5 [pii].

44. Zhang, F.; Hammack, C.; Ogden, S. C.; Cheng, Y.; Lee, E. M.; Wen, Z.; Qian, X.; Nguyen, H. N.; Li, Y.; Yao, B.; Xu, M.; Xu, T.; Chen, L.; Wang, Z.; Feng, H.; Huang, W. K.; Yoon, K. J.; Shan, C.; Huang, L.; Qin, Z.; Christian, K. M.; Shi, P. Y.; Xia, M.; Zheng, W.; Wu, H.; Song, H.; Tang, H.; Ming, G. L.; Jin, P., Molecular signatures associated with ZIKV exposure in human cortical neural progenitors. *Nucleic Acids Res* **2016,** *44*, 8610-20. DOI: gkw765 [pii] 10.1093/nar/gkw765.

45. Qian, X.; Nguyen, H. N.; Song, M. M.; Hadiono, C.; Ogden, S. C.; Hammack, C.; Yao, B.; Hamersky, G. R.; Jacob, F.; Zhong, C.; Yoon, K. J.; Jeang, W.; Lin, L.; Li, Y.; Thakor, J.; Berg, D. A.; Zhang, C.; Kang, E.; Chickering, M.; Nauen, D.; Ho, C. Y.; Wen, Z.; Christian, K. M.; Shi, P. Y.; Maher, B. J.; Wu, H.; Jin, P.; Tang, H.; Song, H.; Ming, G. L., Brain-Region-Specific Organoids Using Mini-bioreactors for Modeling ZIKV Exposure. *Cell* **2016,** *165* (5), 1238-54. DOI: 10.1016/j.cell.2016.04.032 S0092-8674(16)30467-6 [pii].

46. Garcez, P. P.; Loiola, E. C.; Madeiro da Costa, R.; Higa, L. M.; Trindade, P.; Delvecchio, R.; Nascimento, J. M.; Brindeiro, R.; Tanuri, A.; Rehen, S. K., Zika virus impairs growth in human

neurospheres and brain organoids. *Science* **2016,** *352* (6287), 816-8. DOI: 10.1126/science.aaf6116 science.aaf6116 [pii].

47. Qian, X.; Nguyen, H. N.; Jacob, F.; Song, H.; Ming, G. L., Using brain organoids to understand Zika virus-induced microcephaly. *Development* **2017,** *144* (6), 952-957. DOI: 10.1242/dev.140707 144/6/952 [pii].

48. Xu, Y. P.; Qiu, Y.; Zhang, B.; Chen, G.; Chen, Q.; Wang, M.; Mo, F.; Xu, J.; Wu, J.; Zhang, R. R.; Cheng, M. L.; Zhang, N. N.; Lyu, B.; Zhu, W. L.; Wu, M. H.; Ye, Q.; Zhang, D.; Man, J. H.; Li, X. F.; Cui, J.; Xu, Z.; Hu, B.; Zhou, X.; Qin, C. F., Zika virus infection induces RNAi-mediated antiviral immunity in human neural progenitors and brain organoids. *Cell Res* **2019,** *29* (4), 265-273. DOI: 10.1038/s41422-019-0152-9 10.1038/s41422-019-0152-9 [pii].

49. Li, C.; Deng, Y. Q.; Wang, S.; Ma, F.; Aliyari, R.; Huang, X. Y.; Zhang, N. N.; Watanabe, M.; Dong, H. L.; Liu, P.; Li, X. F.; Ye, Q.; Tian, M.; Hong, S.; Fan, J.; Zhao, H.; Li, L.; Vishlaghi, N.; Buth, J. E.; Au, C.; Liu, Y.; Lu, N.; Du, P.; Qin, F. X.; Zhang, B.; Gong, D.; Dai, X.; Sun, R.; Novitch, B. G.; Xu, Z.; Qin, C. F.; Cheng, G., 25-Hydroxycholesterol Protects Host against Zika Virus Infection and Its Associated Microcephaly in a Mouse Model. *Immunity* **2017,** *46* (3), 446-456. DOI: S1074-7613(17)30074-2 [pii] 10.1016/j.immuni.2017.02.012.

50. Yoon, S.-J.; Elahi, L. S.; Pașca, A. M.; Marton, R. M.; Gordon, A.; Revah, O.; Miura, Y.; Walczak, E. M.; Holdgate, G. M.; Fan, H. C.; Huguenard, J. R.; Geschwind, D. H.; Pașca, S. P., Reliability of human cortical organoid generation. *Nature methods* **2019,** *16* (1), 75-78. DOI: 10.1038/s41592-018-0255-0.

51. Zhang, N. N.; Tian, M.; Deng, Y. Q.; Hao, J. N.; Wang, H. J.; Huang, X. Y.; Li, X. F.; Wang, Y. G.; Zhao, L. Z.; Zhang, F. C.; Qin, C. F., Characterization of the contemporary Zika

virus in immunocompetent mice. *Hum Vaccin Immunother* **2016,** *12* (12), 3107-3109. DOI: 10.1080/21645515.2016.1219004.

52. Larocca, R. A.; Abbink, P.; Peron, J. P.; Zanotto, P. M.; Iampietro, M. J.; Badamchi-Zadeh, A.; Boyd, M.; Ng'ang'a, D.; Kirilova, M.; Nityanandam, R.; Mercado, N. B.; Li, Z.; Moseley, E. T.; Bricault, C. A.; Borducchi, E. N.; Giglio, P. B.; Jetton, D.; Neubauer, G.; Nkolola, J. P.; Maxfield, L. F.; De La Barrera, R. A.; Jarman, R. G.; Eckels, K. H.; Michael, N. L.; Thomas, S. J.; Barouch, D. H., Vaccine protection against Zika virus from Brazil. *Nature* **2016,** *536* (7617), 474-8. DOI: nature18952 [pii] 10.1038/nature18952.

53. Boonyasuppayakorn, S.; Reichert, E. D.; Manzano, M.; Nagarajan, K.; Padmanabhan, R., Amodiaquine, an antimalarial drug, inhibits dengue virus type 2 replication and infectivity. *Antiviral Res* **2014,** *106*, 125-34. DOI: 10.1016/j.antiviral.2014.03.014 S0166-3542(14)00088-6 [pii].

54. Lessler, J.; Chaisson, L. H.; Kucirka, L. M.; Bi, Q.; Grantz, K.; Salje, H.; Carcelen, A. C.; Ott, C. T.; Sheffield, J. S.; Ferguson, N. M.; Cummings, D. A.; Metcalf, C. J.; Rodriguez-Barraquer, I., Assessing the global threat from Zika virus. *Science* **2016,** *353* (6300), aaf8160. DOI: 10.1126/science.aaf8160.

55. Lang, Y.; Li, Z.; Li, H., Analysis of Protein-Protein Interactions by Split Luciferase Complementation Assay. *Curr Protoc Toxicol* **2019,** *82* (1), e90. DOI: 10.1002/cptx.90.

TOC: Table of Contents

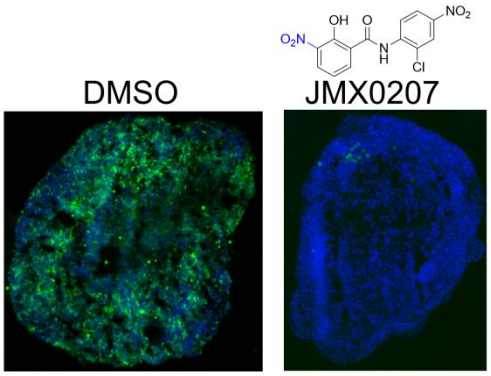

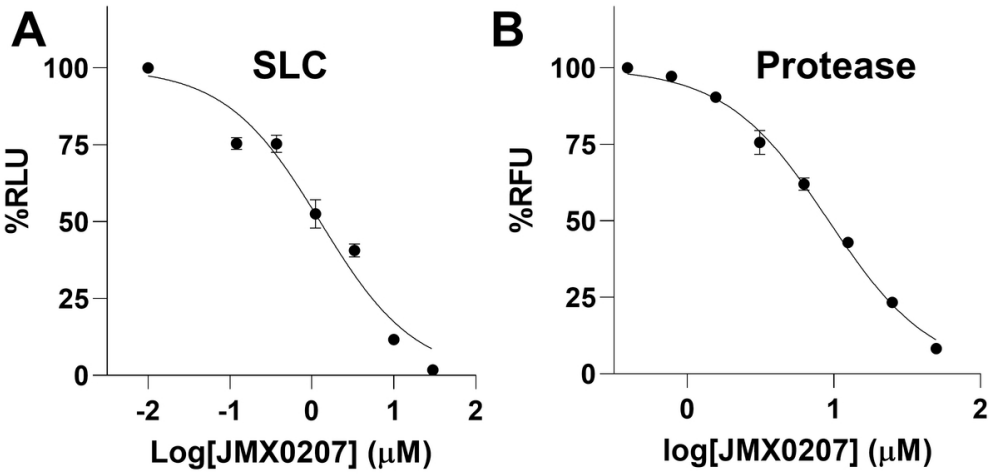

Figure 1. Inhibition of the NS2B-NS3 interactions and protease activity. (A) Dose-dependent inhibition of SLC upon binding of NLuc-NS2B49-66 to GST-CLuc-NS3 by JMX0207. N=3. (B) Dose-response inhibitions of the DENV2 His-NS2B/His-MBP-NS3 protease activity by JMX0207. N=3. In both (A) and (B), DMSO control was set as 100%. The values represent means ± standard deviation (S.D.) in all panels.

101x48mm (300 x 300 DPI)

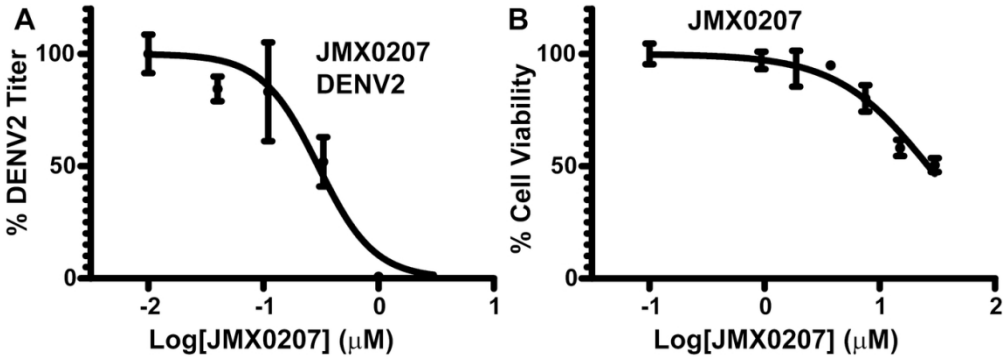

Figure 2. JMX0207 inhibits DENV. (A) Dose-dependent inhibition of DENV2 infectivity by JMX0207. N=3. (B) Cell viability assay. A549 cells were incubated with various concentrations of JMX0207 and then assayed for viability at 48 hrs post-incubation. N=3. Error bars in both panels represent the standard deviations at each concentration.

118x41mm (300 x 300 DPI)

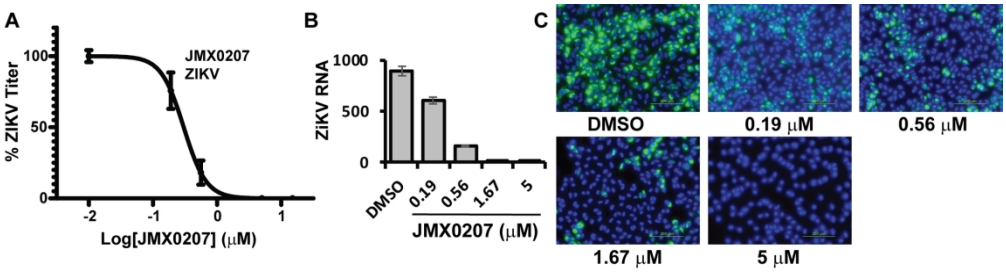

Figure 3. JMX0207 inhibits ZIKV. (A) Dose-dependent inhibition of ZIKV infectivity. N=3. (B) qRT-PCR analysis of inhibition of viral RNA from ZIKV-infected A549 cells by JMX0207. N=3. Error bars in panels (A) and (B) represent the standard deviations at each concentration. (C) Immunofluorescence assay of inhibition of viral protein production by JMX0207, using pan-flavivirus anti-E 4G2 antibody (green) (ATCC).

185x49mm (300 x 300 DPI)

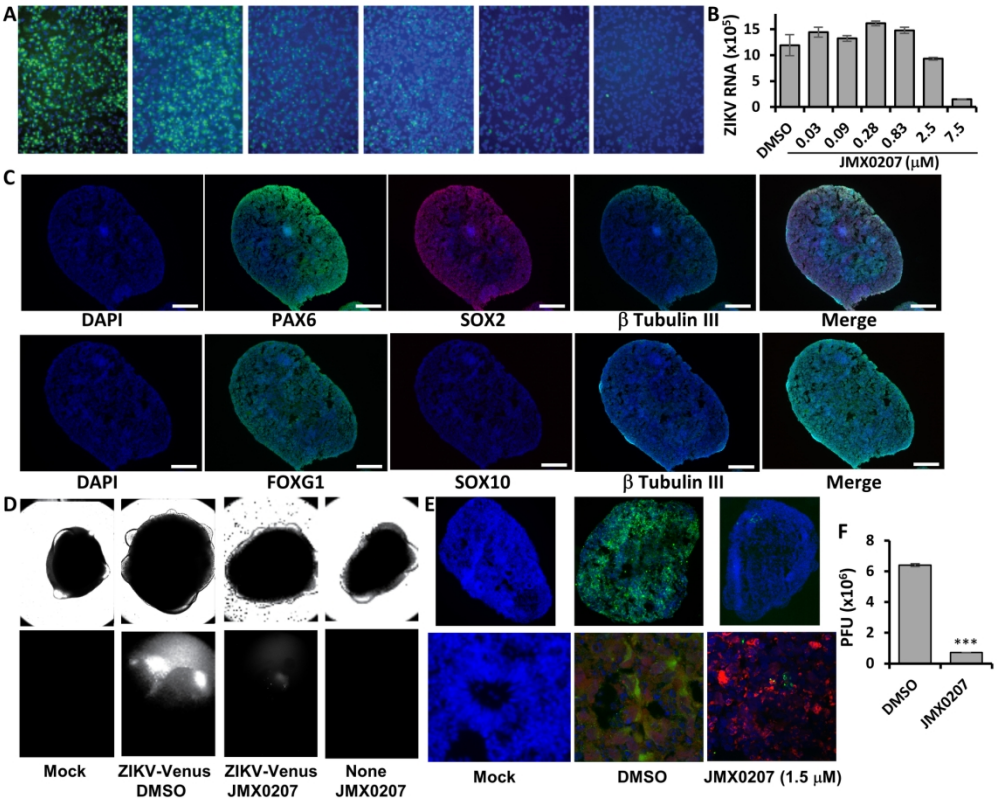

Figure 4. Inhibition of ZIKV in cells relevant to ZIKV. (A) Immunofluorescence assay (IFA) of inhibition of viral protein expression in human neural progenitor cells by JMX0207, using pan-flavivirus anti-E 4G2 antibody (green) (ATCC). Nuclei (blue) was stained in all IFA assays by the Hoechst stain solution. (B) qRT-PCR analyses of inhibition of viral RNA from ZIKV-infected human neural progenitor cell (HNPC) by JMX0207. N=3 (C) ZIKV organoid infected with ZIKV-Venus. The 3D organoids were infected with PBS (Mock), or ZIKV untreated (DMSO), or ZIKV treated with JMX0207, or Mock treated with JMX0207. Upper panel, bright field image of intact organoids. Lower panel, Venus fluorescence image (excitation 515 nm, emission 528 nm) of the intact 3D organoids. (D) Forebrain reginal specification of organoids. Organoids were stained positive for forebrain identity markers PAX6 (green, upper panel), FOXG1 (green, lower panel) and SOX2 (Red (Magenta after merge with DAPI (Blue)), upper panel) at 20 days. The sections were stained positive for general neuronal marker TUJI (cyan, upper and lower panels) and were negative for SOX10 (Red, lower panel). DAPI-merged data were shown. Nuclei (DAPI, Blue); scale bar 200μm. (E) Slices of organoid infected with ZIKV PRVABC59. The 3D organoids were infected with PBS (Mock), or ZIKV untreated (DMSO), or ZIKV treated with JMX0207. Upper panel, IFA using anti-E 4G2 antibody (green); blue, DAPI. Lower panel, details of signature rosette region of the 3D organoids (Mock) or infected region (DMSO/ZIKV and JMX0207/ZIKV). Red: Pax6. (F) ZIKV production from the 3D organoids at 5 dpi. Culture supernatants were collected, and virus production was quantified by PFU assay. N=3. Error bars in panels (B) and (F) represent the standard deviations at each concentration.

171x137mm (300 x 300 DPI)

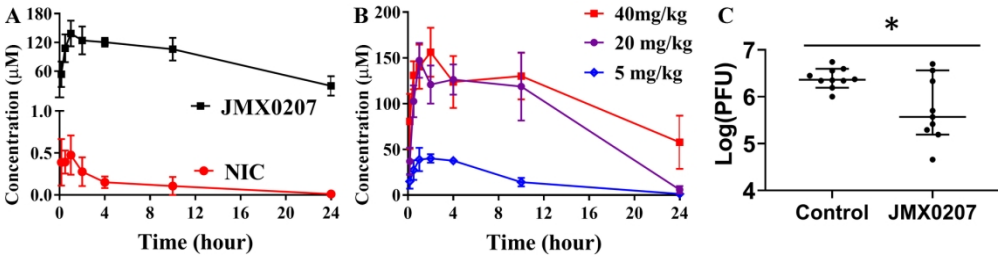

Figure 5. In vivo antiviral activity of JMX0207 against ZIKV. (A) Pharmacokinetic study of niclosamide and JMX0207. Adult female B6 mice were given a single oral dose of either niclosamide or JMX0207 at 40 mg/kg. Plasma was obtained at various times after dosing. Both niclosamide and JMX0207 were extracted from the plasma and then analyzed by LC-MS/MS as described in the Methods. N=4. (B) Pharmacokinetic study of JMX0207 at different doses. N=4-5. The values in panels (A) and (B) represent means ± S.D. (C) Viremia was detected by a plaque forming unit (PFU) assay on day 3 post-infection of ZIKV with a dose of 1.7 × 105 PFU/mouse in four-week-old A129 mice, which were treated with vehicle or JMX0207 though oral gavage. Difference between JMX0207 (N=10) or vehicle (N=10) treatment was analyzed by using the unpaired, two-tailed t-test. *, P=0.0081. Error bars represent data range of median with 95% confidence interval.

169x46mm (300 x 300 DPI)

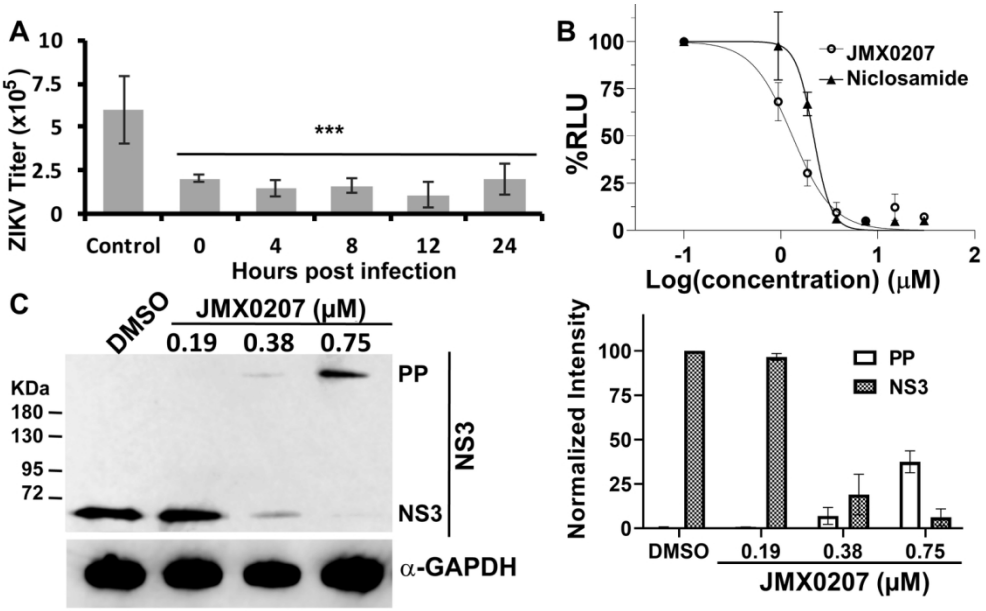

Figure 6. Mechanism of action studies. (A) Time of addition. JMX0207 (0.75 μM) was added at indicated time points post-infection. Viral titers were quantified using plaque forming assay 48 hrs post-infection. DMSO was added to control. N=3. ***, $p<0.001$. (B) Dose-dependent inhibition of DENV2 replicon by niclosamide and JMX0207. N=3. (C) WB analysis of dose response inhibition of ZIKV NS3 production by JMX0207 treatment (left). Right, Band intensities of PP and NS3 normalized to the GAPDH control (N=3). Pre-seeded A549 cells in 6-well plate were treated with JMX0207 or DMSO control and infected with ZIKV with MOI of 0.1, as described previously.21 At 48 hrs post-infection, cells were washed, harvested, and protected by protease inhibitor cocktail prior to lysis by SDS-PAGE loading buffer. Upon incubation at 95 ºC for 10 min, sample was subjected to Western blot analysis with anti-ZIKV NS3 (GTX133309, GeneTex, Inc.) and anti-GAPDH (CB1001, EMD Millipore) as primary antibodies. Error bars in all panels represent the standard deviations at each condition.

136x83mm (300 x 300 DPI)

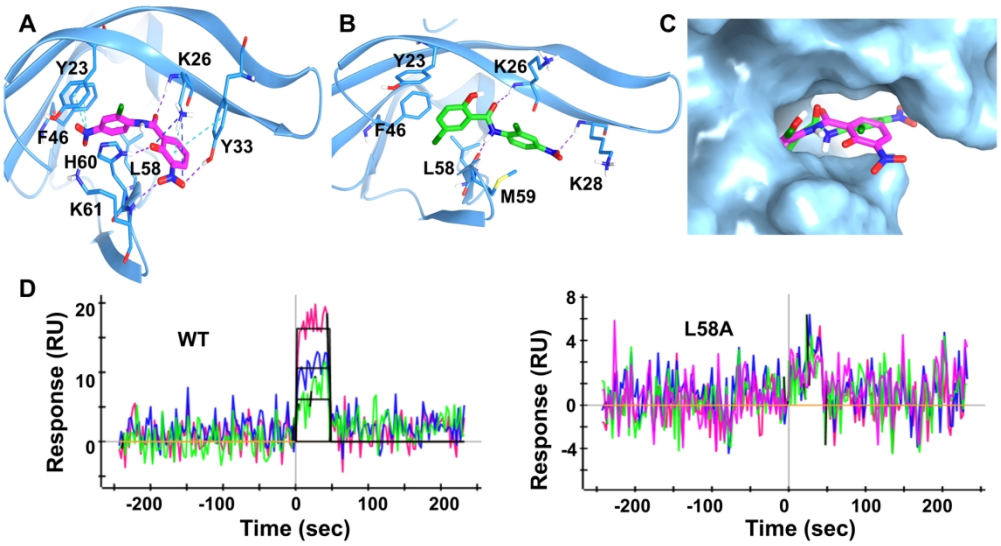

Figure 7: Docking and mutagenesis. (A) Predicted docking pose of JMX0207 (magenta) docking into NS3pro of DENV2 (PDB Code: 2FOM). NS3pro is in blue ribbon representation and binding site key interaction residues are highlighted in stick presentation. π cation and π stacking are shown as cyan dotted lines, H-bond in purple and salt bridge in blue. (B) Predicted binding pose of Niclosamide (green) docked into NS3pro of DENV2. H-bond is shown as purple dotted lines. (C) JMX0207 and Niclosamide superimposed at the predicted binding site, in surface representation. JMX0207 is shown as magenta sticks and Niclosamide in green. (D) Representative SPR analysis of JMX0207 binding to the MBP-NS3 protease wild-type and mutant L58A.

172x93mm (300 x 300 DPI)